Impermeabilization of carbon black-based smart coatings for strain-sensing purposes

Gabriele Milone[1*], Christos Vlachakis[1], Jean-Marc Tulliani[2] and Abir Al-Tabbaa[1]

[1] *Department of Engineering, University of Cambridge, Trumpington Street, Cambridge CB2 1PZ, UK*

[2] *Department of Applied Science and Technology, INSTM R.U. Lince Laboratory, Politecnico di Torino, Corso Duca degli Abruzzi 24, Turin 10129, Italy*

Abstract

This study explores self-sensing properties in carbon black (CB)-based cementitious coatings, focusing on the influence of internal moisture on electrical measurements. Various saturation levels were examined by gradually drying the coatings and encapsulating them with epoxy resin to shield them from external humidity. Results show that inner water impacts the strain-sensing response of the coating, reaching an optimal moisture saturation of 25% where an equilibrium between carbon black particles, water, and free ions was attained. For coatings on tension surfaces of concrete beams under flexural loads, 230.7 ± 25.8 was the obtained gauge factor for 3 wt% added carbon black. Epoxy-sealing reduced the bonding strength between the coating and the substrate by 27%. Nonetheless, epoxy-encapsulated coatings with 3 wt% carbon black achieved a gauge factor of 110.9 ± 35.5, indicating a promising path for the production and application of self-sensing coatings that remain unaffected by external humidity conditions.

Keywords: Structural health monitoring, self-sensing, carbon black, cement-based materials, smart coatings

1. Introduction

As the construction industry has shifted its focus towards preventive and predictive maintenance, strategies to extend the lifespan of existing structures are being explored [1].

*Corresponding author
Email address: gm683@cam.ac.uk

Structural health monitoring (SHM) aims to manage and evaluate the conditions of structures through data acquisition and analysis obtained through external sensors and visual analysis [2]. Traditional methods for monitoring structural integrity, however, face issues related to cost, accessibility, and real-time data acquisition [3]. While these SHM techniques are commonly used, a significant drawback in their practical implementation involves their effectiveness in challenging environments. These conditions may affect their performance, potentially resulting in early failures, and consequently, insufficient data collection and structural evaluation [4]. To overcome these limitations, innovative monitoring solutions have emerged, including the use of smart materials [5]. Among them, self-sensing composites exploit the electrical conductivity obtained by incorporating carbon-based nanomaterials, such as Carbon Black (CB), into the cement mixture [6], [7], [8], [9]. Thus, these composites can correlate changes in electrical resistivity with mechanical stresses and deformations within structures, allowing for the autonomous and real-time detection of structural issues [10]. This sensing property can be further processed and interpreted to monitor additional conditions such as the presence of damage in the structure [11]. In addition, the initiation of corrosion can be detected by monitoring strain development from swelling of steel reinforcement [12]. Alternatively, the electric charge storage capability of these materials has been employed for de-icing and snow-melting purposes [13] or to attenuate and shield electromagnetic radiation [14].

The system's conductivity primarily arises from ionic conduction, due to the presence of absorbed water, and from the movements of electrons within the filler network, i.e., electronic conduction [15]. The latter mechanism depends on the proximity and contact between conductive particles, as a continuous filler network facilitates electron movement [9]. Thus, the variation in filler distance, which can be related to a change in its concentration and distribution throughout the matrix, strongly influences the conduction mechanism [16]. Ionic conduction in Portland cement binders, on the other hand, is primarily attributed to hydroxide and

sodium/potassium/calcium ions in the pore solution [17]. Different from electronic conduction, the ionic conductive process is highly dependent on the amount of free water present in the matrix. Therefore, assuming a sufficient filler presence, a reduction in the inner water concentration makes the cementitious specimen more dependent on electronic conduction, i.e., electronically dominant. In contrast, saturated conditions produce a highly conductive sample – prevalently ionic – whose electric network does not primarily rely on the presence of conductive fillers. This phenomenon leads to electronic/electrolytic interactions and the formation of Electrical Double Layers (EDL) at the interfaces [18], [19], [20]. Thus, as stated by Zhang *et al.* [21], the overall electrical response of conductive cement derives from a function of four conductive pathways involving ionic, electronic and EDL of electrolytic solution with both cement and conductive particles.

Researchers have noted a correlation between the strain-sensing properties of cementitious composites and internal moisture levels. Han *et al.* [22] demonstrated that high water-to-cement (w/c) ratios have been observed to improve the gauge factor. Indeed, large w/c, leading to more extended porous networks, is assumed to increase the system's deformation capacity while improving the filler dispersion [23]. Moreover, Dong *et al.* [24] found an increasing trend in the sensing response of carbon black-based systems, i.e., gauge factor varying between 400 and 485 within 0-8% range of water content. However, as moisture levels increased further, the composites' strain sensitivity decreased to 150. Similarly, del Moral *et al.* [25] identified a diminishing gauge factor beyond a saturation degree of 75% for CBT/graphite-based elements. Han *et al.* [26] also reported an increase in sensing performance for CNT-based cement composites between 0-3% water content, ranging from 0.6 kΩ/MPa to 0.73 kΩ/MPa. This performance was followed by a decrement, reaching 0.06 kΩ/MPa at 10% water content. Relative humidity (RH) has also been acknowledged as a factor influencing the sensing performance of cementitious materials by increasing the specimens' inner moisture. Kim *et al.*

76 e] reported an increase in stress sensitivity from 0.060 to 0.079%/MPa as the relative humidity
77 increased from 20% to 60%, before decreasing to 0.064%/MPa for RH = 80%.

78 The aforementioned analyses can be justified by the balance between inner moisture content
79 and the presence of conductive fillers [28]. In fully saturated systems, filler particles become
80 water coated, resulting in minimal changes to the electrical characteristics of the composite
81 network when subjected to mechanical stress [29]. During the drying process, on the other
82 hand, the absence of water reduces the overall ionic conductivity [30]. **Table 1** presents a list
83 of optimal saturation degrees found in the literature in relation to the obtained sensitivity to
84 external load. In consideration of the above information, it can be suggested that peak
85 sensitivity is not necessarily attained by completely dried samples. A certain level of water
86 content is beneficial for sensing as it facilitates tunnelling effects within the matrix, enhancing
87 the electric network [25]. The optimal moisture content, however, appears to vary depending
88 on the type and concentration of conductive phase in the cementitious composite. In addition,
89 these tests are typically conducted in a laboratory where, differently from real-case
90 applications, environmental conditions are controlled and are stable throughout the sensors'
91 lifespan.

92 **Table 1** – Optimal saturation degrees and relative strain/stress sensitivity found in the
93 literature. The optimal saturation degree values reported for [24], [30] were calculated with
94 available data in the papers.

Article	Conductive filler type	Filler concentration	Optimal saturation degree [%]	Strain / stress sensitivity
[31]	Carbon nanotubes	0.5 wt%	55	8%/MPa
[24]	Carbon black	3 wt%	40	488
[32]	Conductive brass fibres	0.8 vol%	91	28
[30]	Carbon nanofibres	2.5 vol%	63	101.3

[25]	Carbon nanotubes / Graphite	1 wt% / 5 wt%	71	3.8

The above-mentioned studies described the monitoring behaviour in varying humidity conditions of self-sensing materials directly subjected to external load, namely *bulk applications* [5], [28], [33]. On the other hand, externally attached cementitious sensors, designed as *coating applications*, offer versatile use for both new and existing structures [34], [35]. These sensors not only present cost benefits [36] but are also characterised by broader monitoring capabilities than conventional sensing mechanisms (e.g., strain gauges). Traditional sensing devices generally encounter issues related to limited lifespan, decreased sensitivity, and inadequate compatibility with the concrete substrate [37], [38]. In contrast, cement-based coatings have emerged as cost-effective alternatives, demonstrating good compatibility with concrete and greater versatility in monitoring – ranging from strain detection [39] to damage identification and tomography [40]. Moreover, beyond their primary monitoring function, external cementitious sensors also serve as an effective retrofitting solution, capable of addressing both structural and non-structural repairs [41]. Therefore, this study aims to investigate how moisture influences the strain-monitoring capability of self-sensing CB-based coatings on concrete substrates subjected to bending.

Despite the advancements characterising self-sensing materials, a few challenges remain in maintaining consistent performance in varying environmental conditions. As the theory behind self-sensing materials is based on multiple conductive mechanisms [21], [28], [42], [43], maintaining consistent moisture levels in aggressive environments [30] is critical to ensuring a stable sensor response [44], [45], [46]. The implementation of waterproofing measures is acknowledged as an effective approach to safeguard general cementitious composites from moisture ingress [29], [32], [47], [48]. Dong *et al.* [49] impermeabilized carbon black-based cementitious binders with the addition of silicon hydrophobic powder and crystalline waterproofing admixture. That said, the use of such mineral admixtures can affect the electrical

network inside the matrix, therefore, altering its sensing properties. Alternatively, the sensing system can be externally sealed with a resin layer, keeping the internal properties constant and ensuring no interference from environmental conditions [50], [51]. Similarly, in the field of road construction, epoxy membranes can be used for the impermeabilization and protection of infrastructure from multiple aggressive agents [48], [52], [53].

Hence, this study advances the state of the art by focusing on an effective and efficient impermeabilization protocol for carbon black-based smart coatings. Indeed, differently from previous studies which focused mainly on bulk applications, without addressing the challenges of encapsulation, this research develops an impermeabilization solution to enhance the durability and reliability of external cementitious sensors. Through the application of waterproof epoxy resin, which is both a safe and simple method for encapsulation, the stabilisation of the sensor's electrical reading can be achieved in changing conditions, providing a possible solution for practical real-world requirements. The monitoring efficacy of externally applied coatings relies on their interaction with the substrate [54]. Consequently, the presence of a polymeric layer negatively affects the interface between the two [55]. This can lead to critical strain differences [56], diminishing the monitoring property of the sensor. Therefore, with the aim of ensuring a robust interfacial bond when investigating the sensing performance of smart coatings [57], [58], this work also focuses on the adhesion strength variation caused by epoxy gluing and its impact on the sensing performance of impermeabilized smart coatings.

In summary, this work examines the influence of different internal moisture conditions on CB-based smart coatings. After determining the optimal saturation degree, epoxy encapsulation was used to stabilise the water content in the sensors while shielding them from external humidity. The objective of this work is to provide a sensing solution that can be applied as a coating without hindering the mechanical properties of the structural elements under study.

Despite a weaker strain propagation, the epoxy-sealing protocol demonstrated consistency and reliability in the sensing response. The obtained trade-off between moisture control and sensing reliability highlights the potential of these systems for monitoring civil engineering structures and expanding the scope of structural health monitoring.

2. Materials and Methods

2.1 Materials

Smart coatings were produced by mixing Portland cement (CEM I – 52.5N), supplied by Hanson Cement, UK and conforming to BS EN 197-1 standard [59], with compressed acetylene carbon black powder (**Table 2**), supplied by Thermo Fisher Scientific, UK. To aid the mixing procedure, different percentages of superplasticizer, MasterGlenium C315 – supplied by BASF, UK – were applied by weight of carbon black, providing consistent workability for the varying CB concentrations investigated.

Table 2 – Carbon black properties as per the manufacturer.

Appearance (colour)	Black
Form	Powder
Ash (%)	≤0.50
Electrical resistivity (Ω·cm)	≤0.25
pH	7.6
Moisture (%)	0.12
Average particle size (nm)	42
Surface area (m^2/g)	75
Bulk density (g/L)	170-230

In view of practical applications of smart coatings, this study focused on concrete substrates as a reference for most of the infrastructural environment. The substrate was fabricated by blending sand and coarse aggregate with the cement mix (conforming to BS EN 206-1 standard [60]). The sand had a 2 mm maximum size, a specific gravity of 2.56, and 0.6% water absorption, while the coarse aggregate had an 11 mm maximum size, a specific gravity of 2.58, and 1.8% water absorption, consistent with prior research [61]. The coarse aggregate size was

chosen in agreement with standard BS EN 12390-1 [62] as the maximum dimension for laboratory size applications. Moreover, coarse aggregates have the potential to increase the interaction between the concrete substrate and carbon-based coatings. Indeed, when employing repair layers on concrete substrates, failure occurs at the interfacial transition zone between the two phases [63]. Thus, the presence of coarse aggregates, by enhancing friction and interlocking effect between the two, facilitates the deposition of cementitious overlays and modifies the failure modes [64], [65].

To secure and affix the coatings onto the concrete substrates, a two-part epoxy resin, *Araldite*® *rapid resin* from Huntsman Advanced Materials, US and supplied by RS Components, UK, was brushed on the coating's surface with one single layer ~0.2 mm thick, which is assumed to impart the greatest lap shear strength for construction applications [66]. The two-phase rapid-hardening adhesive was characterised by a specific gravity of ~1.18, a viscosity of 25-50 Pa.s at 25°C and a pot life of 5-8 minutes. Subsequently, 20 mm in length and 1 mm in thickness copper wires, sourced from RS Components, UK, were incorporated within the coating to ensure stable electrical connectivity throughout the system.

2.2 Sample preparation

This study focused on the strain monitoring of concrete beams (40 mm × 40 mm × 160 mm) with the use of electrically conductive CB-cement paste coatings (7.5 mm × 3 mm × 80 mm). Additionally, this research also highlighted the limits that the epoxy-driven application has on the adhesion strength between carbon black-based pastes (40 mm × 20 mm × 40 mm) and mortar specimens of equivalent size. The sensors' geometry was optimized in relationship to the substrate [67]. Future work could focus on improving the coating's connection by adapting its geometry to match the areal or torsional stiffness of the substrate under study.

2.2.1 Cementitious substrates

The mix design used for producing cementitious substrates, in the form of concrete (BS EN 206-1 [60]), is shown in **Table 3** and followed a cement:water:sand:coarse aggregate ratio of 1:0.45:2.1:3. A laboratory bench-scale blender was used for all mixes which were cast into steel moulds previously sprayed with release oil. The concrete beams' dimensions (i.e., 40 mm × 40 mm × 160 mm) were chosen in agreement with similar works on flexural strain-sensing systems [27], [68]. The samples were compacted for 2 minutes on a vibrating table to release entrapped air and ensure adequate compaction. The specimens were then wrapped in plastic and demoulded after 24 hours. After that, the hardened samples were left to cure at a temperature of 20°C ± 2°C in a water tank for 28 days.

Table 3 – Mix design of the concrete substrate tested in this study (kg/m^3).

	Cement	Water	Fine aggregate	Coarse aggregate
Concrete substrate	395	178	829	1184

The concrete beams were reinforced with a 200 mm long Ø6 mm rebar, with a cover depth of 10 mm, to improve their mechanical performance under flexural loading. The rebar diameter was selected according to the minimum longitudinal reinforcement of concrete set by the standards (BS EN 1992-1 [69]). Additionally, this research investigated the adhesion influence that epoxy has on the bond between cementitious substrates and carbon-based samples. A series of mortar 40 mm × 20 mm × 40 mm prisms were cast, demoulded and cured analogously to the aforementioned 40 mm × 40 mm × 160 mm prisms. **Table 4** presents the mix design used for producing mortar substrates (BS EN 998-1 [70]), with a cement:water:sand ratio of 1:0.45:3. Differently from the sensor response evaluation to strain, the adhesion test involved mortar specimens as the cubic sample size proved to be unsuitable for concrete casting, according to BS EN 12390-1 [62].

The cement-polymer interaction primarily relies on the connection between the polymer oxygen-groups and hydration products [55], [71], [72]. Hence, water has the ability to weaken and disrupt this connection [71]. Since mortar has lower water absorption than concrete [73], due to lower volume of aggregates [74], it is plausible that it retains a larger amount of water on its surface. Thus, mortar was assumed to be characterised by a weaker interaction with the polymer. On the other hand, concrete surfaces demonstrated an enhanced interlocking effect with epoxy resin, attributed to the micro-voids and roughness characterising its surface [75], [76]. Therefore, the use of mortar helped determine critical parameters influencing epoxy-driven adhesion between two cementitious composites, as the interaction with the polymeric resin is assumed to be weaker in mortar than in concrete [77], [78].

Table 4 – Mix design of the mortar substrate tested in this study (kg/m^3).

	Cement	Water	Fine aggregate
Mortar substrate	479	216	1437

2.2.2 Conductive sensor coatings

The cementitious conductive sensors were fabricated with a water-to-cement ratio of 0.45 and varying filler content of 2, 3 and 4% by weight of cement (**Table 5**), labelled in the manuscript as CB2, CB3 and CB4, respectively. The studied concentrations of carbon black, along with the production, size, curing and application protocols for the samples, were developed in agreement with previous work from the authors [67].

Table 5 – Mix design of the coating composition tested in this study (kg/m^3).

Name	Cement	Water	Carbon black	Dispersant	CB dosage [wt%]	CB dosage [vol%]
CB2	2921.2	1327.5	57.8	5.8	2.0	11.1
CB3	2906.8		85.9	8.6	3.0	15.7
CB4	2892.4		113.5	11.3	4.0	19.9

The sensing coatings were produced by initially blending the carbon black powder with half of the mixing water and superplasticizer. The CB-based solution was mechanically stirred via a rw20 mixing probe (IKA, UK) at 4000 rpm for 6 minutes. Subsequently, cement was introduced into the homogeneous solution along with the remaining water, and mechanical stirring continued for 5 minutes at 5000 rpm until achieving sufficient homogeneity for casting. The casting and consequent curing techniques varied based on the application protocol, which is discussed in the following section. For the sensing coatings, the electrodes (i.e., copper wires) were vertically embedded in the coatings, aided by small pincers that controlled their position and prevented any movement throughout the casting and curing phases. The locations of the electrodes were chosen to represent the entire constant bending moment region (i.e., 60 mm).

2.2.3 Coating application protocol

Two types of application methodologies are introduced in this section, i.e., fresh and epoxy-driven. The influence of both coating installation procedures was investigated in relation to adhesion strength and electromechanical analysis. The fresh application protocol is schematically represented in **Figure 1a**, for CB-based coatings. This consisted of casting the fresh conductive CB-based mix on three hours old concrete prisms to ensure robust adhesion between the two elements. The coating + substrate systems were subsequently sealed in plastic film and removed after 24 hours. They were afterwards left to cure for 28 days by being submerged in water (**Figure 1b**), in agreement with BS EN 13670 [79] and BS 8500 [80]. After curing, the samples underwent a progressive drying protocol to be investigated at specific saturation degrees, as described in section 2.3.2.

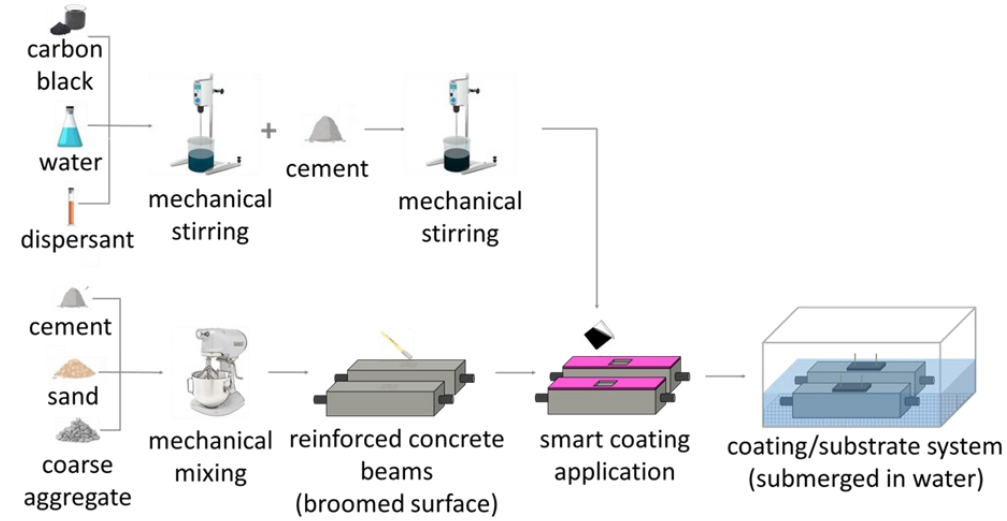

(a)

(b)

Figure 1 – (a) Schematic representation of the mixing steps of CB-cement paste coatings and concrete substrates. First, concrete is mixed and cast in 40 mm × 40 mm × 160 mm moulds. After 3 hours, the conductive CB/cement mixture is produced and applied on top of the concrete substrate in 7.5 mm × 3 mm × 80 mm silicon moulds. Finally, the (b) composite system is left to cure in water for 28 days.

In regard to the epoxy-driven method, as illustrated in **Figure 2a**, both the conductive coatings and the concrete substrates were cast separately and submerged in water for 28 days. Afterwards, the fully cured coatings were dried at a specific saturation degree (section 2.3.2) and subsequently sealed with epoxy (**Figure 2b**). Finally, the carbon black-based sensors were bonded to 28-day old concrete substrates (**Figure 2c**) using the same polymeric resin. To ensure

good contact between the coatings and the substrates, the entire system was pressed with a constant weight for 24 hours. The coating + epoxy + substrate systems were tested in bending and the influence of epoxy on the sensor's electrical response was obtained and compared with that of the coating + substrate systems for the same saturation degree.

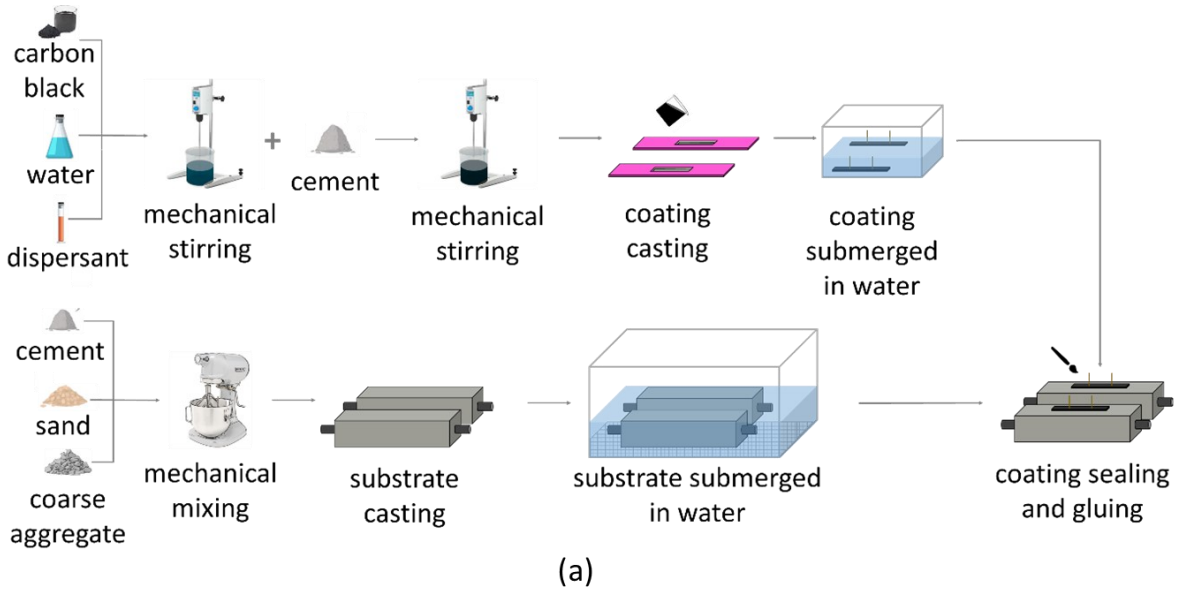


(b)

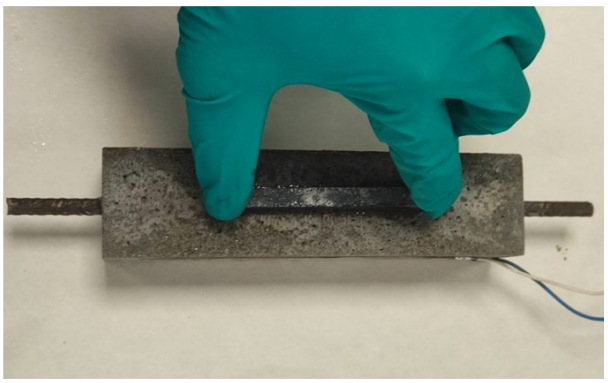
(c)

Figure 2 – (a) schematic representation of the enhanced application method for CB-cement paste coatings onto concrete substrates. Concrete is mixed and cast in 40 mm × 40 mm × 160 mm moulds and, after 24 hours, left to cure in water. In parallel conductive CB/cement mixture is poured in 7.5 mm × 3 mm × 80 mm silicon moulds and left to cure for one day before being submerged in water. Finally, the sensing coating is (b) sealed with epoxy and (c) accordingly glued to the hardened substrate.

2.3 Experimental program

2.3.1 Adhesion strength

Splitting tensile bond tests were conducted to assess the adhesion strength between the concrete substrate and the smart coating. Both the coating/epoxy/substrate and coating/substrate interfaces were investigated following the same fabrication technique as the bending test described in the previous section. Adhesion was assessed by the splitting tensile test on 40 mm cubic samples, these samples comprised two halves: CB-cement paste and mortar (**Figure 3**). This test was conducted for both the fresh and epoxy driven application methods, as schematically depicted in **Figure 3 a,b**. Moreover, since epoxy may reduce the bond strength between the two elements, adhesion was also assessed following a similar configuration while incorporating a 15 mm × 5 mm × 15 mm indentation in the prism with carbon black addition (**Figure 3 c,d**).

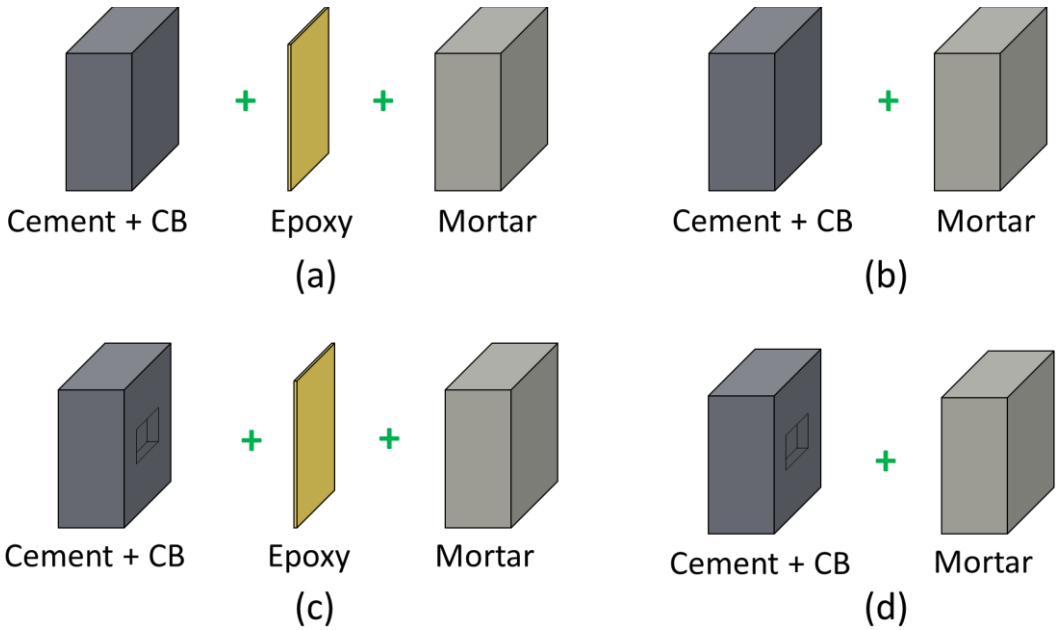

Figure 3 – Schematic description of samples tested (a,c) with and (b,d) without epoxy interface between mortar and CB-based conductive cement. Samples (c,d) represent the 5 mm deep indentation in the CB-based section.

285 The bond strength was evaluated according to equation 1 by employing a load rate of 500 N/s.
286 The obtained values for all configurations were compared and evaluated accordingly.

287 $$f_{ct} = \frac{2F}{\pi L d} \quad \text{(eq. 1)}$$

288 where f_{ct} [MPa] is the bond strength, F [N] is the load at failure, L [mm] is the load length and
289 d [mm] is the height of the tested element (BS EN 12390-6 [81]). Similar to the bending test,
290 the bond strength was defined by testing three identical cubic samples.

291 2.3.2 Drying protocol

292 To investigate the influence of moisture content on the electrical response of the carbon black-
293 based systems, the specimens were subjected to a controlled saturation and subsequent gradual
294 drying regimen, during which both electromechanical response and mass were measured at
295 specific time intervals. This technique was employed due to its simplicity and equipment
296 availability to indirectly assess moisture content in combination with electrochemical
297 impedance spectroscopy which validated any variation in the water conductive phase within
298 the sample. The drying protocol is depicted as a flowchart in **Figure 4**.

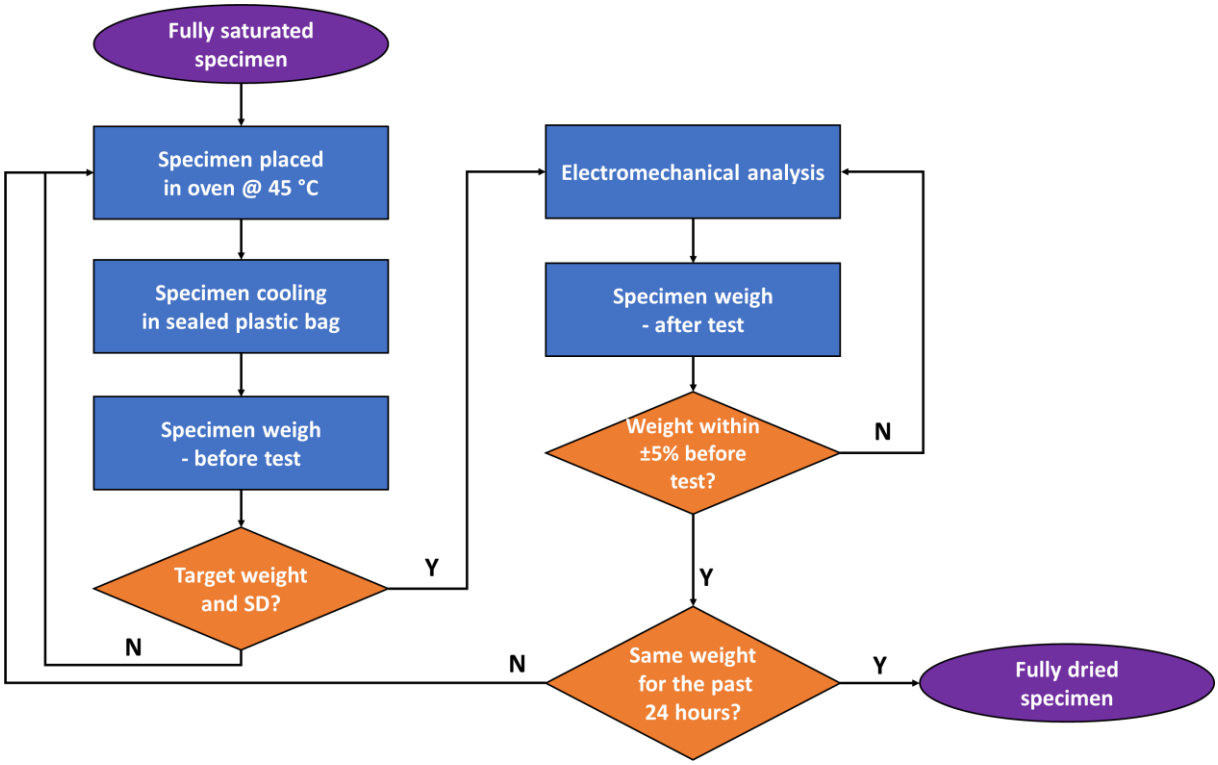

299

300 **Figure 4** – Flowchart showing the steps in the drying protocol and moisture characterisation
301 for strain sensing testing.

302 The initial step involved the saturation of the specimens with water, followed by a systematic
303 desiccation process where the weight was constantly measured to ensure stable inner moisture
304 for the duration of the sensing test. Water-saturated specimens were placed in an oven with a
305 constant temperature of 45°C to ensure the evaporation of moisture until the target weight was
306 reached. The drying temperature and duration were based on preliminary experiments,
307 achieving effective cement drying while avoiding rapid evaporation of inner water, which
308 would lead to internal stress accumulation [82] and impact the strain monitoring performance
309 of the sensors. Following the drying period, each sample was extracted from the chamber and
310 placed in a sealed plastic bag for approximately 4 hours to prevent moisture exchange with the
311 surroundings. The system was able to cool under laboratory conditions (20 ± 5°C, RH = 50%)
312 until both internal and surface temperatures equilibrated with the laboratory environment. This
313 step was critical in ensuring that no high temperature would affect the electrical properties of

the conductive system (i.e., Seebeck effect [83]). Ultimately, a sample was considered dried when no mass change was witnessed between two consecutive days of oven-drying. The moisture content at a specific time interval was quantified using equation 2 [29]:

$$M_i(\%) = \frac{W_i - W_{dry}}{W_{dry}} \quad \text{(eq. 2)}$$

where W_i is the sample weight at a specific instant (i) and W_{dry} is the weight of a fully dried specimen. In agreement with Zhang *et al.* [21], the saturation degree was calculated as:

$$SD_i(\%) = \frac{M_i}{M_{sat}} \quad \text{(eq. 3)}$$

where M_i is the moisture content at an instant i and M_{sat} is the moisture content for fully saturated specimens. Finally, the electromechanical tests were conducted on samples at saturation degrees of 90%, 75%, 50% and 25%. The investigated saturation degree interval was considered suitable to cover realistic working conditions of self-sensing specimens [21]. At the end of each strain-sensing test, the weight of the specimen was measured to ensure that the change in the system's moisture was less than 5%. Preliminary tests were also developed towards both fully saturated (SD = 100%) and dried (SD = 0%) configurations. Nonetheless, these conditions were not investigated in this study as it was unfeasible to maintain such saturations for the entire duration of the test.

For instance, fully saturated samples rapidly released some of the inner moisture to the surrounding environment during the duration of the test. Indeed, the rapid moisture equilibrium dynamics occurring inside the materials led the samples to adapt to the surrounding environment. On the other hand, the complete drying of specimens led to thermal expansion and, consequently, fractures within the specimens' microstructure. Moreover, preliminary sensing tests with very low saturation degrees showed no consistent electrical response and, consequently, this configuration was not considered any further.

To address these issues, future work could investigate the influence of implementing different drying and moisture stabilisation methods to the microstructural integrity of the conductive system. Possible solutions involve slower drying rate or the use of chemical desiccation protocols [84]. Additionally, future studies could modify the duration and frequency of the sensing test to reduce moisture fluctuation during the experiment; potential modifications include adjusting the loading rate or reducing the number of loading cycles. For instance, increasing the load speed can help reduce testing time and decrease the moisture variability. However, the loading rate should be designed to ensure compatibility with the data collection frequency, not to impact the sensor's resolution. Alternatively, the specimens could be preconditioned at an earlier stage and subsequently placed in a humidity chamber to correct any moisture variation before being reloaded for a shorter duration.

2.3.3 Electromechanical test

Once the specific saturation degree was achieved for all specimens, the sensor response evaluation to strain was conducted. The prismatic samples were subjected to external flexural load within their elastic domain. The application of flexural load for strength and sensing tests was accomplished with an Advantest9 Uniframe machine – supplied by CONTROLS, Italy. A 4-point bending test, with a loading rate of 50 N/s, was used to determine the flexural strength of 40 mm × 40 mm × 160 mm prisms of CB-cement paste (**Figure 5**) according to equation 4:

$$f_b = \frac{3}{4}\frac{PL}{bd^2} \quad \text{(eq. 4)}$$

where f_b [MPa] is the flexural strength, P [N] is the maximum load at failure, L [mm] is the support span, b [mm] is the width of the test beam and d [mm] is the depth of the beam. The flexural strength was obtained by testing three identical samples for each carbon black dosage to provide statistical confidence in the measurements.

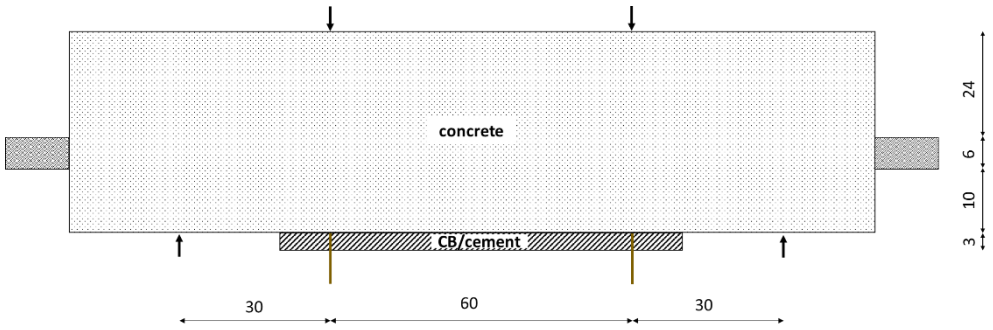

361

362 **Figure 5** – Experimental setup for electromechanical testing of a concrete beam with
363 conductive coating (all units in mm). The coating is here shown with some transparency to
364 better present the embedment of the copper wires used as electrodes.

365 Via 2-probe method [85], [86], the application of alternate current was implemented using a
366 potentiostat PGSTAT204 (Metrohm, Switzerland) to minimise the polarization effect in the
367 system. The voltage amplitude of 0.5 V was selected as the optimal value for sinusoidal signal
368 to ensure a stable and linear response within the system [87], aligning with previous studies
369 [88], [89], which have demonstrated its effectiveness in perturbing cementitious binders.
370 Regarding the frequency range (between 20 Hz – 300 kHz at 9 points per decade), the upper
371 limit was chosen to ensure a stable electrochemical impedance response from the equipment,
372 avoiding instrumental and environmental noise at higher frequencies. The lower frequency
373 limit, on the other hand, was selected to adequately capture the Nyquist plot's low-frequency
374 region without significantly increasing the measuring time. Preliminary frequency analyses
375 between 1 Hz and 300 kHz were significantly more time-consuming and did not yield
376 additional useful information compared to the chosen range. The bulk resistance, obtained by
377 deconvoluting the impedance spectrum, can be used to define the effective conductivity,
378 defined by equation 5:

379 $$\frac{1}{R_{bulk}} \left(\frac{L}{A}\right) = \sigma_{bulk} \qquad \text{(eq. 5)}$$

380 where R_{bulk} is the resistance value corresponding to the ionic conduction of the interconnected
381 pores in parallel with the electronic conduction through the conductive filler [21] [Ω], L is the

distance between the pair of chosen electrodes or gauge length [m] and A is the cross-section of the specimen [m^2]. The findings detailed in Section 3.1 showed the significance of ionic conduction in contributing to the electrical response.

After assessing the electrical properties, this study evaluated the strain sensing response of the coatings by measuring changes in their resistivity under applied loads. This is referred to as the Fractional Change in electrical Resistivity (FCR) [90]. Within the elastic range, 20 load cycles were applied to cementitious prisms as displayed in **Figure 6**. The load ranged between 0.84 MPa (0.6 kN) to 4 MPa (2.84 kN), with a loading rate of 50 N/s, all within a standard laboratory setting. The minimum and maximum thresholds represented 5% and 20% of the substrate's flexural strength, respectively. The maximum load was selected to ensure bending within the sample's elastic region. The preload was chosen to produce irreversible minor damage in the coating, enhancing the sensor's response amplitude to external load [91]. The number of cycles was chosen as the electric output tended to stabilize due to polarization drift and drying of trapped water. Consequently, the assessment of load sensitivity focused on the last 5 cycles, where a stable sensing response was attained. The electromechanical study involved three carbon black concentrations (i.e., 2, 3 and 4 wt%) each at four different saturation levels, i.e., 90%, 75%, 50%, and 25%.

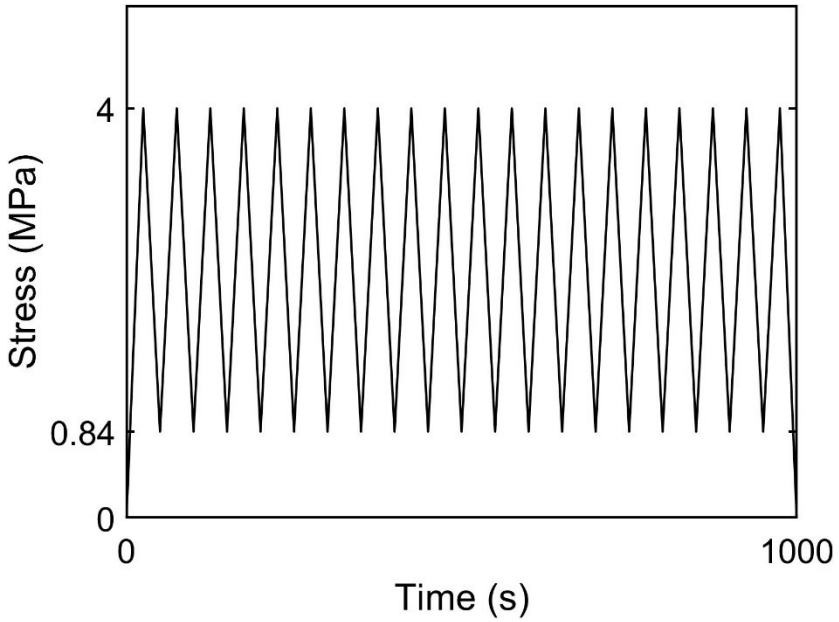

399

400 **Figure 6** – Graphical representation of 20 loading cycles applied to concrete prisms and
401 ranging between 0.84 MPa (0.6 kN) to 4 MPa (2.84 kN), over 1000 seconds with a loading
402 rate of 50 N/s.

403 The strain value (ε) at the midpoint of the concrete beam was precisely determined using
404 Digital Image Correlation (DIC) with GeoPIV-RG [92]. When subjected to external loads, the
405 relationship between FCR and the induced strain can be defined using equation 6.

406 $$FCR = \frac{\rho - \rho_0}{\rho_0} = \lambda \cdot \varepsilon \qquad \text{(eq. 6)}$$

407 where ρ is the instantaneous resistivity, which is a function of the state of strain and the
408 conductive filler, ρ_0 is the initial resistivity value (i.e., when no load is applied) which depends
409 mainly on the conductive filler, ε is the strain and λ is the angular coefficient of the FCR-ε
410 curve. Ultimately, the strain sensitivity was determined through the gradient of the linear
411 regression applied to the FCR versus strain plot. This sensitivity is defined as the fractional
412 change in resistance per unit strain, commonly referred to as the gauge factor (GF).

3 Results and discussion

3.1 Saturation degree influence on strain-sensitivity

This section discusses the flexural strain response of smart coatings applied on concrete prisms in bending at four different saturation degrees (SD): 90%, 75%, 50% and 25%. In this case, the coatings were not sealed from external environments and their application technique is described in **Figure 1**.

The FCR amplitude in each strain cycle correlates with the coating's strain sensitivity, as demonstrated in **Figure 7**, which compares the electrical response of smart coatings for varying saturation degrees against the strain development in the concrete substrate's bottom layer. The obtained measurements were related to the micromechanical behaviour of functional fillers getting strained inside the partially insulating matrix [93]. Self-sensing materials in bending typically present both increase and decrease in the FCR, however, given the localised application of the sensor, the piezoresistive response was only characterised by a resistance increment due to the progressive stretching and separation of conductive particles for each loading cycle, before returning to almost initial conditions when unloaded [5].

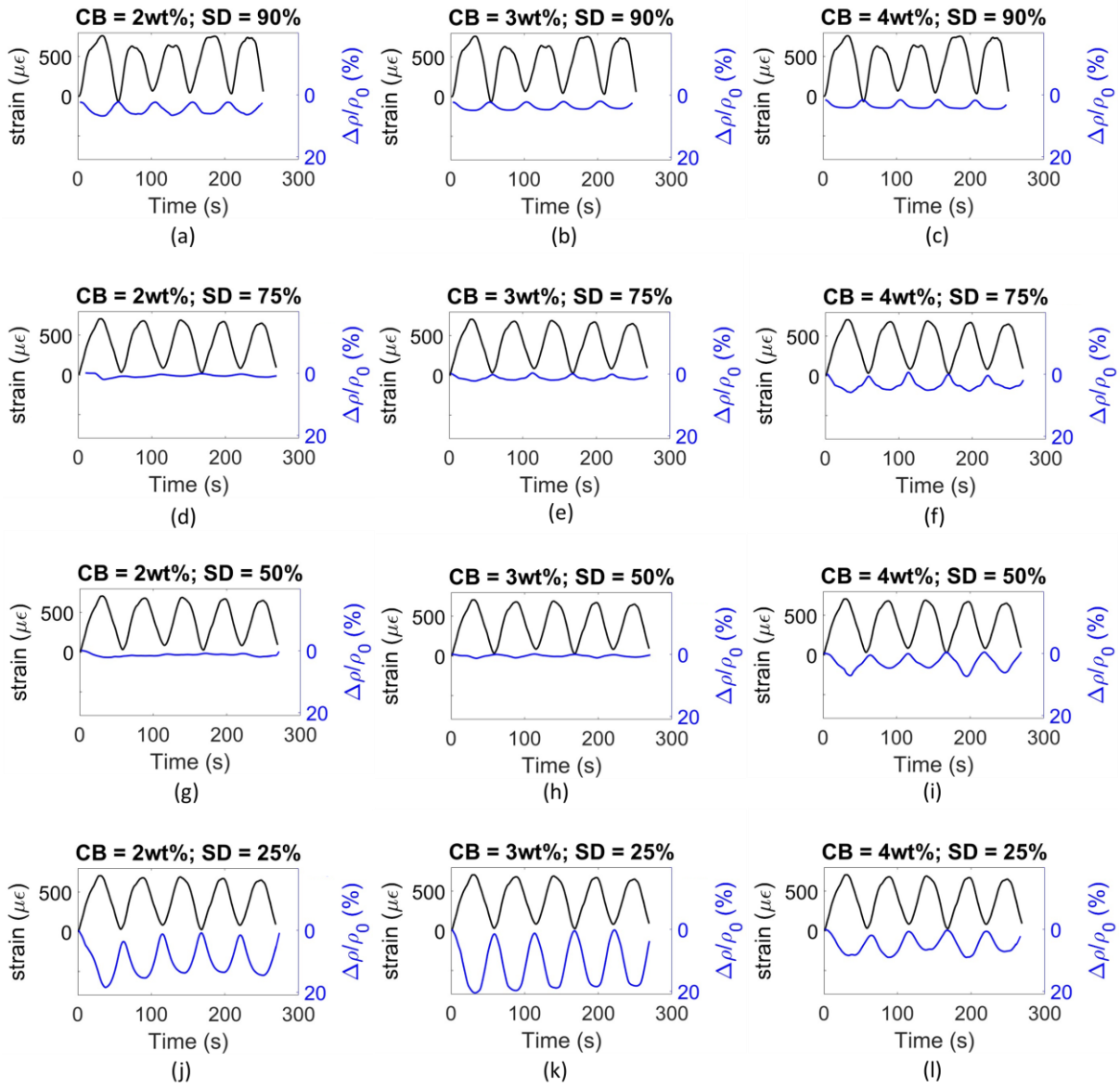

Figure 7 – Strain and FCR time histories for (a,d,g,j) CB2, (b,e,h,k) CB3, and (c,f,i,l) CB4 smart coatings, applied on partially reinforced concrete beams subjected to cyclic flexural loading. Each configuration was tested at a constant saturation degree of (a,b,c) 90%, (d,e,f) 75%, (g,h,i) 50% and (j,k,l) 25%.

The strain sensing test analysis in **Figure 8** reveals the various trends across different saturation degrees. In agreement with equation 6, the linear fit for all loading cycles (black line and blue dots in **Figure 8**) provided the gauge factor and coefficient of correlation. For cementitious composites containing 2 and 3 wt% of carbon filler, the gauge factor gradually decreased as SD reduced from 90% ($GF_{2wt\%} = 55.5 \pm 6.0$ and $GF_{3wt\%} = 39.1 \pm 5.7$) to 50%

438 ($GF_{2wt\%}$ = 10.1 ± 1.5 and $GF_{3wt\%}$ = 11.4 ± 1.6). However, the strain sensitivity peaked at
439 SD = 25% for both dosages reaching a maximum of 168.1 ± 45.6 and 230.7 ± 25.8 for CB2
440 and CB3 respectively. In contrast, cementitious composites with 4 wt% of conductive additive
441 exhibited a progressive increase in the gauge factor, starting from a minimum value of
442 35.9 ± 2.5 at 90% to a maximum of 101.4 ± 10.1 for SD = 25%. The fractures developed in the
443 microstructure at each loading cycle can influence the conductive network of the matrix, and
444 consequently its response to strain, particularly in samples with low inner water content
445 (SD = 25%).

446 Additionally, minor fluctuations in internal moisture (<5%) during electromechanical testing,
447 although impacting all measurements, significantly affected samples with higher FCR
448 responsiveness. These variations were quantified by weighing the specimens immediately
449 before and after the electromechanical test to provide an accurate measure of internal moisture
450 (**Figure 4**). To minimise the impact of moisture fluctuations on the electrical performance, and,
451 consequently, strain-sensitivity, possible measures include conducting the electromechanical
452 test within a controlled environmental chamber or applying a more robust moisture barrier [25],
453 [94].

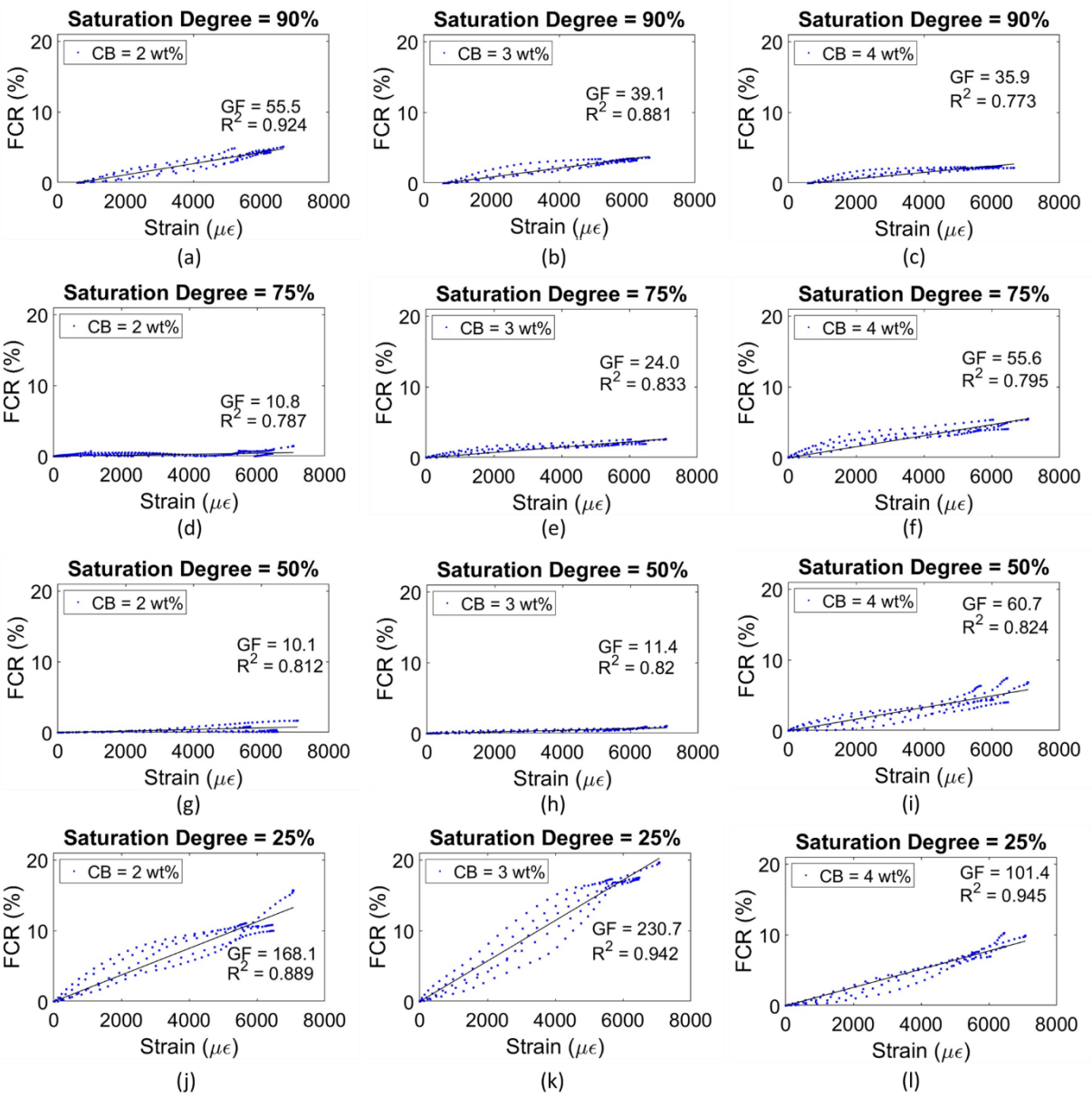

454

455 **Figure 8** - FCR vs strain for substrates/coatings subjected to monotonic flexural load (last 5
456 loading cycles), and linear fit models, as a function of varying CB dosage: (a,d,g,j) 2 wt%;
457 (b,e,h,k) 3 wt%; and (c,f,i,l) 4 wt%. Saturation degree = (a,b,c) 90%; (d,e,f) 75%; (g,h,i) 50%;
458 and (j,k,l) 25%.

459 **Figure 9** summarises the trend for flexural gauge factor as a function of saturation degree and
460 carbon black dosage. Coatings with nearly exclusive electronic conduction (SD = 25%)
461 exhibited the highest sensitivity to external loads, yet gauge factor trends varied with CB
462 concentrations. This behaviour was attributed to the bulk conduction mechanism and
463 ionic/electronic balance within the matrix [15], [95]. Increasing the filler content can enhance

464 the moisture dependency of bulk conductivity through a rise in the solid-liquid interfaces. This
465 effect, however, can be reduced by a high filler content which mitigates short-circuiting
466 because of numerous particle contact points [21].

467 For samples with filler inclusion at 2 and 3 wt%, a growing presence of capillary water
468 disrupted electronic conduction between CB particles, resulting in a decreased gauge factor
469 [32]. Indeed, high conduction did not necessarily correspond to an analogous sensing property.
470 In contrast, the low conductivity achieved by cementitious samples with 2 and 3 wt% of CB
471 produced a highly unstable electrical network which was significantly influenced by any
472 strain/stress variation. Since the effect of moisture on the sensing performance of coatings is
473 limited, the obtained response can be discussed in comparison with bulk applications. For
474 instance, Dong *et al.* [24] subjected cement paste cubes with 3 wt% CB addition to 3 cycles of
475 compressive loading up to 2 MPa. The highest FCR magnitude of 12% was achieved for
476 samples with a water content of 8%, and the maximum FCR progressively decreased as the
477 water content increased. Similarly, in this study, a decrease in FCR was observed as the
478 saturation degree increased. However, at partially saturated conditions (i.e., 90%), CB2 and
479 CB3 coatings exhibited a recovery in strain sensitivity, with maximum FCR amplitudes of
480 5.4 ± 0.4 and 4.8 ± 0.6, respectively.

481 When using a low filler dosage, a higher water presence modified the percolation zone,
482 significantly relying on ionic conduction contribution. It could be posited that the electric
483 network in the matrix, due to the low filler concentrations, benefitted from a large presence of
484 water which contributed to an ionically dominant conductive network. Wang *et al.* [30] found
485 a similar pattern when including 2.5 vol% carbon nanofibres in mortar samples subjected to
486 cyclic compressive loading. Applying 5 MPa corresponded to a maximum FCR amplitude of
487 2% for a water content of 1.5%, which led to a gauge factor of 84.8. As moisture content
488 increased to 2.64% the gauge factor decreased to 29.9. Del Moral *et al.* [25] found an analogous

strain sensitivity trend for cement pastes including 1 wt% CNT subjected to multiple compressive loading cycles with a 4.06 MPa stress amplitude. For low saturation degrees, they obtained an FCR variation of 8%, corresponding to a gauge factor of ~3.2, followed by a sharp decrement for wetter conditions (25% < SD < 50%). Similar to the findings presented in this study, for large inner water concentrations, the gauge factor began a progressive increment, peaking at the saturation degree of 71%.

In contrast, the 4 wt% CB dosage reached a balance between ionic and electronic conduction mechanisms, maintaining a relatively stable micromechanical performance as the material dried. A similar pattern was observed by Wen & Chung [19], who tested the strain sensing response of carbon fibre-based cement pastes in wet and dry conditions. They found that when applying σ_c = 2.5 MPa to specimens with a filler concentration of 0.5 wt%, the gauge factor decreased from 276 under dry conditions to 220 under wet conditions. This behaviour, in agreement with percolation theory, can be attributed to the abundant presence of conductive filler, which guaranteed uninterrupted electronic connections throughout the matrix and, therefore, a lower and more linear dependence on moisture [28].

Therefore, higher saturation degrees decreased strain sensitivity as excessive moisture overly stabilizes the conductive network. Consistent findings were obtained by Dong *et al.* [49], who found that submerging cement pastes with 1 wt% CB in water for 24 hours decreased the composite's piezoresistive response. When compressively loaded up to 5 MPa, CB-based samples experienced a variation in the FCR amplitude from 40% to 25%, before and after saturation respectively. The addition of large amounts of filler increases the porous network and water channel [96], which, in turn, increases the electrical conductivity but decreases the strain sensitivity [97].

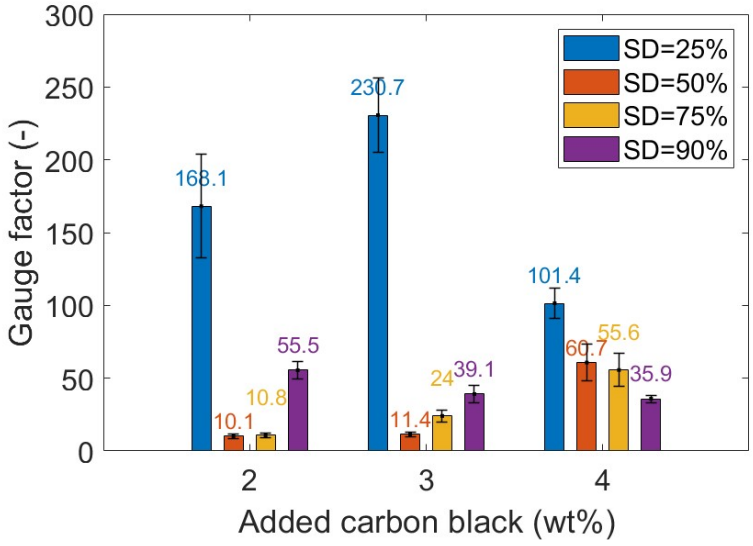

512

513 **Figure 9** – The gauge factor for 2, 3 and 4% CB dosage in the cement–based coating for
514 varying saturation degree (i.e., 25, 50, 75 and 90%). The standard deviation was defined by
515 comparing gauge factors of samples with the same filler concentration and inner moisture
516 content. Refer to online version for colour representation.

517 By interpreting the logarithmic Nyquist plots in **Figure 10**, which depict cementitious pastes
518 with varying carbon black dosages at different saturation degrees, the transition in the
519 water/filler conduction mechanisms becomes evident. An equivalent circuit can be defined
520 from the interaction between the contact resistance of the electrodes and the capacitance and
521 resistance of the pore solution, cement paste and conductive fillers [98]. The first semicircle
522 can be deconvoluted into the contribution of electrical double layer (EDL) between cement and
523 the electrolytic solution, ionic conduction and electron hopping [42], [99]. The mid-arc is
524 related to the EDL between conductive particles and electrolytic solution [100], [101], [102]
525 while the Warburg line at low frequencies is associated with the electrode/electrolyte
526 interaction [42], [103], [104].

527 Thus, for all three filler concentrations, the Warburg line disappeared as the influence of water
528 progressively reduced. Consequently, the first and mid arcs were characterised by a descending
529 electrical resistance. Indeed, when water evaporates, the resistance/conductance of the pore

530 solution is substituted by insulating air [15], [99], leading to less conductive pathways [105].
531 The imaginary part of the impedance (*-Z''*) behaved similarly. Nonetheless, its decrement was
532 smaller for higher carbon black dosages. This proved that the electrical capacitance and
533 polarization effect were particularly influential in the strain sensing performance for coatings
534 with lower filler additions [30]. Indeed, at high filler concentrations (e.g., 4 wt%), there is a
535 lower dependence on moisture because there is a stable and mutual conductive bulk-cluster
536 pathway amongst the particles [28]. In addition, the obtained results showed that EIS has the
537 potential for continuous in-situ monitoring of moisture under varying environmental
538 conditions. This technique can help deconvoluting the contributions of various conductive
539 phases within cementitious matrices, offering a real-time and non-destructive method to
540 monitor changes in internal water content. However, this type of application presents several
541 challenges, including the need for preliminary sensor calibration and robust application of the
542 coating to withstand harsh environments. Additionally, the integration of real-time data
543 analysis and wireless data transmission for remote monitoring would necessitate significant
544 electronic optimisation before any practical implementations.

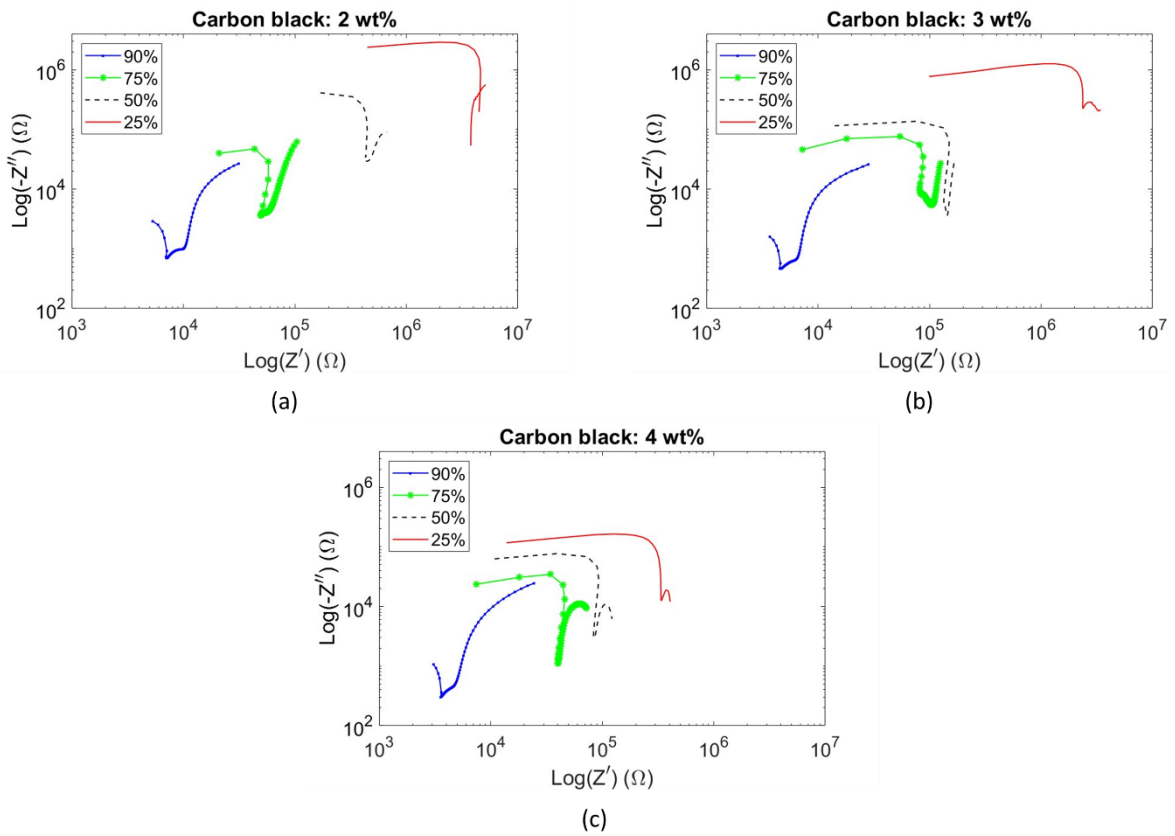

545

546 **Figure 10** – Nyquist logarithmic plots for (a) CB2, (b) CB3 and CB4 (c), at a frequency range
547 of 1 Hz – 10^6 Hz, as a function of saturation degree: 90%; 75%; 50%; and 25%. All systems at
548 high inner water content displayed three semi-circles that progressively reduce to two as the
549 moisture decreases and the electrical contribution of the free water reduces [106].

550 When considering large inner water concentrations, coatings with 2 wt% of filler reached
551 maximum sensitivity under flexural strain. However, this study has proven that coatings with
552 3 wt% carbon black can reach the highest gauge factor performance in partially dried settings.
553 Therefore, this mix design was selected for future tests, ensuring all experiments were
554 conducted at the optimal saturation degree of 25%. Nonetheless, the obtained empirical trends
555 can only be partially interpreted theoretically via percolative interaction between water and
556 conductive fillers. Therefore, future work will focus on simulations at the nanoscale to better
557 frame the contribution of each phase to the electronic transport mechanism, refining percolation
558 theory for practical applications in water-dependant settings.

559 ***3.2 Epoxy encapsulation***

560 Since this study focused on exploiting the strain-sensing properties of carbon black based smart
561 coatings, the epoxy encapsulation becomes a critical step to be analysed to deduce its influence
562 on the adhesion strength and subsequent contribution to the sensor's electrical response to
563 strain.

564 3.2.1 Adhesion strength

565 This section examined epoxy adhesive's impact on bond strength between a mortar substrate
566 and smart coating using a 40 mm cube. The adhesion results for all configurations of carbon-
567 based cement paste and mortar are depicted in **Figure 11**.

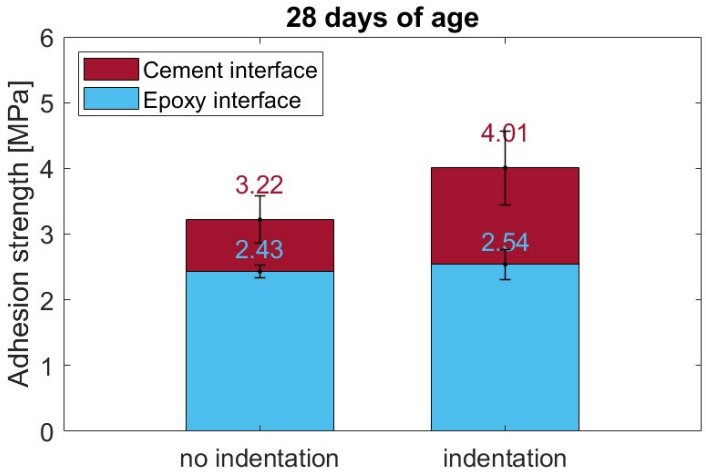

568

569 **Figure 11** – Adhesion strength of 40 mm × 20 mm × 40 mm prisms (CB-based paste and
570 mortar) bonded with and without epoxy adhesive. The x-axis represents the presence of a
571 15 mm × 5 mm × 15 mm indentation on the carbon black paste. Refer to online version for
572 colour representation.

573 The results present a clear variation between the system with and without epoxy bonding. The
574 use of polymeric resin led to a bond strength decrement of approximately 27% with respect to
575 cement-cement interaction. This behaviour agreed with existing cases on repair and
576 strengthening techniques, where the presence of an interstitial section reduces the overall
577 adhesion strength [55], [107]. Nonetheless, the obtained strength of 2.43 MPa was still

578 considered serviceable according to BS EN 1504-3 [108], therefore its adhesive potential could
579 be used for strain-sensing purposes. In addition, for systems with epoxy interface, the presence
580 of the indentation caused a negligible 4% increment in the bond strength. Such a variation was
581 around 25% for samples presenting the indentation with no epoxy gluing. Indeed, the bonding
582 agent acted as a plane of separation between the two halves [109], regardless of any possible
583 benefit from the indentation.

584 It could be posited that the moisture on the two surfaces led to water interference between the
585 bonding agent and the cementitious prisms [110]. Moreover, reduced surface roughness is an
586 additional factor that can affect the epoxy compatibility with cement paste and concrete [111].
587 Indeed, when gluing two cementitious sections, epoxy polymers flatten their surface,
588 diminishing the importance of their superficial roughness [107] and interlocking effect [72].
589 This, combined with moisture, is influenced by the polymeric chains of the resin which struggle
590 to adhere to the C-S-H when loaded. Finally, epoxy interaction with coating and substrate is
591 affected by its shrinkage. Similar to cement-to-cement applications, differential volumetric
592 variations between the various phases can diminish the adhesive potential of the resin, leading
593 to micro-voids and cracks at the interface [112]. To overcome these limitations, both
594 mechanical and chemical surface treatment methods can be employed to modify the surface
595 texture and chemistry, promoting better interaction and strain transfer between the sensing
596 coating and the substrate [113]. Potential techniques include pre-drying the application surface
597 [114] and/or using surface roughening methods [115], which improve the overall adhesion
598 performance of epoxy. However, these techniques were not used to better simulate real-case
599 applications with sensing systems applied directly to untreated substrates.

600 To further improve the bonding capability of the polymeric encapsulation, future studies could
601 focus on employing a specific bonding agent [116]. While epoxy resins are widely recognized
602 for their adhesion properties with cement [55], alternative encapsulation materials, such as

603 silane [117] and decane carboxylic acid [118], can be used as protective layers for cement,
604 reducing hydrophilicity and inhibiting water ingress in C-S-H capillary pores [119].
605 Additionally, using a more ductile impermeabilization layer would benefit the sensing
606 coating's design, particularly when loading the system within its plastic domain.

607 Future work shall address the limited long-term durability and stability of the resin when
608 subjected to external conditions. Indeed, UV exposure [121], thermal variations [122] and
609 chemical attacks [123] can mechanically and chemically deteriorate the sealing structure,
610 failing its protecting purpose. To mitigate these effects, antioxidants, photostabilizers and heat
611 stabilizers could be employed to protect the resin from oxidation, light and thermal-driven
612 degradation [120]. Additional research is required to enhance the impermeabilization durability
613 through long-term field testing and accelerated aging studies.

614 3.2.2 Sensor response evaluation

615 Based on the investigation in section 3.1, all coatings with a saturation degree of 25% resulted
616 in the highest strain-sensing performance for their respective concentration e.g. 2, 3 and 4 wt%.
617 As a result, these sensors were sealed at this specific moisture level and attached to the concrete
618 substrates with epoxy. Their sensing capabilities under 4-point bending within the elastic
619 domain were further explored. **Figure 12** displays the electrical behaviour of the sensing
620 coating under cyclic loading while **Figure 13** represents the FCR of each different coating
621 plotted against the tensile strain of the bottom side of the substrate.

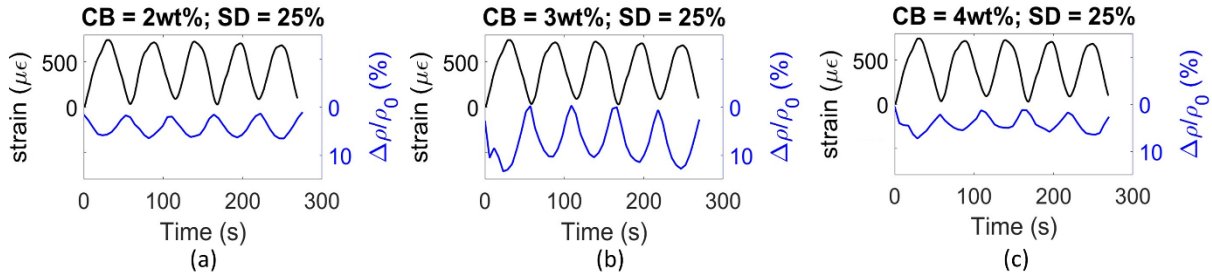

622

623 **Figure 12** – FCR and strain time histories for epoxy sealed CB-based coatings with (a) 2, (b)
624 3 and (c) 4 wt% filler dosage.

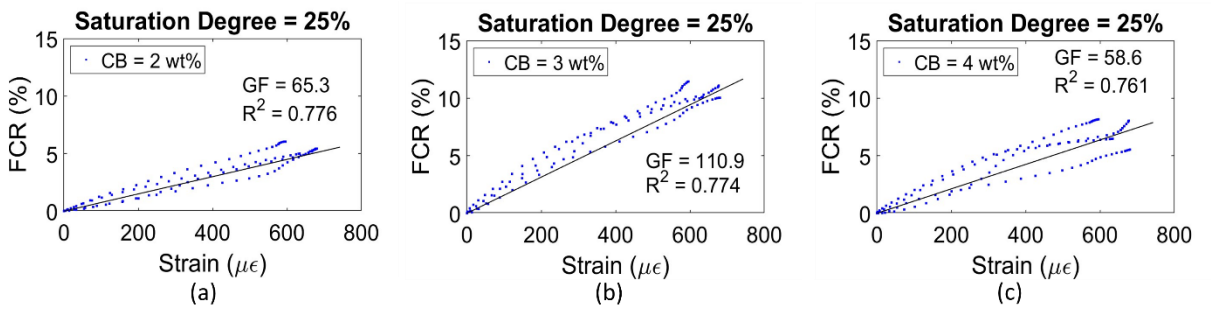

625

626 **Figure 13** – Electric response of epoxy sealed sensing coatings plotted against the tensile strain
627 of the concrete substrate: (a) CB2; (b) CB3; and (c) CB4.

628 **Figure 14** displays the gauge factor for both sealed and unsealed coatings, at a constant
629 saturation degree of 25%. When comparing the obtained sensitivities with the performance of
630 directly cast coatings at the same SD, all epoxy-applied samples witnessed an average
631 decrement in their strain sensitivity of 52 ± 9%. Such a performance was attributed to the epoxy
632 layer between the coating and the substrate and the subsequent interaction weakening in this
633 three-phase system, i.e., sensing coating, epoxy adhesive and concrete substrate. Indeed, using
634 epoxy adhesive for traditional concrete strain gauge measurements introduces variations due
635 to its thickness and curing conditions [56]. The presence of a soft adhesive causes a strain
636 redistribution which in turn results in a lower strain transfer to the sensor [124]. This epoxy-
637 driven installation resulted in an average 25 ± 6% adhesion reduction (**Figure 11**) which, in

638 turn, led to lower gauge factors for the studied CB-based sensing coatings; specifically,
639 65.3 ± 4.3 for CB2, 110.9 ± 35.5 for CB3 and 58.6 ± 6.4 for CB4.

640 This ascending/descending trend was similar to what was defined in the literature by Li & Li
641 [125]. They investigated CB-based mortar specimens, obtaining gauge factors of 52, 247 and
642 105 for 2.5, 5.0 and 10.0 vol% filler concentration, respectively. This descending trend was
643 attributed to the variation of the tunnelling effect and percolation phenomena inside the matrix
644 for increasing carbon black concentrations [47]. Higher dosages of conductive fillers led to a
645 denser network that became less responsive to any load variation [5]. When comparing the
646 obtained gauge factors (**Figure 14**) with carbon black-based bulk applications in compression,
647 e.g., 95 [126], 96 [127], 111 [128], they presented slightly higher sensitivities to CB2 and CB4
648 but were similar to CB3. For externally applied coatings in bending, Baeza *et al.* [129] reported
649 a gauge factor of 64.8. Further studies used the FCR amplitude as a metric to evaluate the
650 sensing performance. In this study, this value reached 6.1, 8.2 and 4.8, for carbon black dosages
651 of 2, 3 and 4 wt%, respectively. Within the literature, Wen & Chung [68] obtained a maximum
652 FCR in tension of 0.15%. Kim *et al.* [27] reported an amplitude of 2% while Durairaj *et al.*
653 [130] noted values between 10-15%. Overall, the maximum FCR values of this work were
654 within range of those found in the existing literature. It should be mentioned though that limited
655 information could be extracted from this value alone and sensing coefficients are a more
656 suitable approach to characterising sensors.

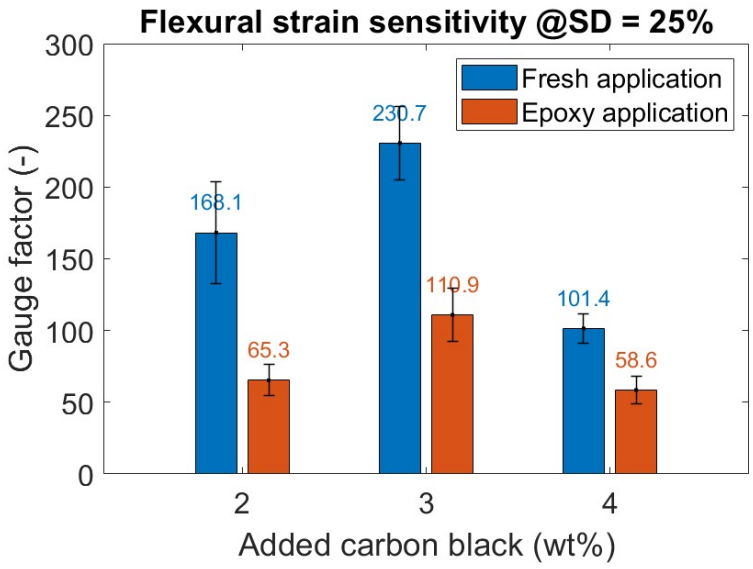

657

658 **Figure 14** – Strain sensitivity for coatings with (*Epoxy application*) and without (*Fresh*
659 *application*) epoxy gluing onto the concrete substrates. Values shown for 2, 3 and 4% CB
660 dosage in the cement–based coating ensuring a constant saturation degree for all specimens of
661 25%. The standard deviation was defined by comparing the gauge factors of samples with same
662 filler concentration and installation protocol. Refer to online version for colour representation.

663 To summarise, in view of structural monitoring for existing structures, epoxy-driven adhesion
664 becomes essential to ensure the durability of the sensing coating on the area under monitoring.
665 Particularly in scenarios where a fresh sensing layer is applied to a substrate that has already
666 undergone its drying and shrinkage phase, the absence of an epoxy coating could result in the
667 early detachment of the smart coating. The use of epoxy resin, however, led to a reduced bond
668 strength between the CB paste and substrate. Since the monitoring capability of externally
669 applied coatings is primarily dependent on their interaction with the substrate [54], a poorer
670 interface between the two led to significant strain differences [56] which in turn caused a
671 reduction in the strain-sensing property. Despite this reduced interaction, employing epoxy
672 impermeabilization results as a highly necessary step for stabilising the impact of water on the
673 system's conduction mechanism and, therefore, its strain sensitivity. Moreover, the obtained
674 electrical response was within the same range of values described in the literature for bulk
675 applications in compression and for coatings in bending.

In conclusion, this study has described the development and installation protocol of a CB-based smart coating capable of providing a reliable and stable sensing measurement. Additional studies are required to assess the performance of the moisture-sealed system when fracture occurs in the substrate and propagates to the coating itself. Extreme damage in the coating is expected to fracture the epoxy layer and lead to a subsequent sudden increase in electrical resistance, providing a critical warning sign of significant fracture extension. Potentially, epoxy could be replaced with a more ductile polymeric resin capable of stretching, tailoring its stiffness to break and influence the electrical response at specific serviceability or ultimate limit states, critical for the parenting structure under study. Experimental approaches could include real-time monitoring of electrical resistance during controlled fracture tests [11], while analytical methods could involve finite element or lattice modelling at the microscale to predict the behaviour of the smart coating under various stress conditions [131]. Hence, future work shall also examine the long-term limitations of smart coatings in relation to the durability and stability of polymeric encapsulation.

4 Conclusions

This study investigated the influence of inner moisture on the electrical properties and strain-sensing characteristics of carbon black-based cementitious coatings applied onto concrete substrates. Different saturation degrees were considered for coatings attached to the surface of the substrate and encapsulated in epoxy resin to seal the inner humidity.

The following conclusions were drawn from the results and discussions presented in this study:

- An optimal saturation degree for the system was defined at 25% where a balance between carbon black particles, water and free ions was achieved, significantly enhancing the strain-sensing response.

- The maximum gauge factor for sensing coatings attached on the tension surface of concrete beams subjected to elastic flexural load was 168.1 ± 45.6 for 2 wt%, 230.7 ± 25.8 for 3 wt% and 101.4 ± 10.1 for 4 wt% of added carbon black.
- Epoxy-driven sealing, while reducing the adhesion strength by 27% (2.43 MPa) compared to cement-on-cement interfaces, effectively impermeabilized the sensing system, stabilising its electrical properties.
- Despite halving the strain-sensing capabilities, epoxy-encapsulated sensing coatings presented gauge factors comparable to conventional sensors (i.e., $GF_{2wt\%} = 65.3 \pm 4.3$, $GF_{3wt\%} = 110.9 \pm 35.5$ and $GF_{4wt\%} = 58.6 \pm 6.4$), underscoring their potential in structural health monitoring.

In summary, the interplay between inner water and conductive fillers significantly influences the electrical properties and strain sensing behaviour of cementitious composites. Although epoxy encapsulation reduces mechanical bonding strength, it is crucial for controlling moisture and maintaining a stable sensor performance. This study has confirmed that achieving optimal moisture/filler balance is crucial to maximising strain sensitivity. Therefore, standardising the design and application protocol for CB-based coatings through effective epoxy encapsulation ensures stable and consistent strain-sensitivity in different environmental conditions, across the designed sensing life. The coatings investigated in this study demonstrated how smart materials can be used to enhance the longevity and safety of various structure types when compared to conventional sensors. Possible large-scale field analysis could employ the smart coatings described in this study, providing both moisture control and sensing monitoring. This application ensures that the strain sensors, applied across the structure's most critical sections, maintain stable performance regardless of external environmental conditions. Additionally, reference sensors could be deployed for any necessary compensations in electrical readings. Future studies will focus on optimizing these smart sensors for broader applications, including

damage sensing and corrosion monitoring. Indeed, when loading the system within its plastic domain, a stable water concentration is maintained through the epoxy encapsulation. This stability in electrical properties can be exploited for the continuous monitoring of crack initiation and propagation at the substrate level, further extending the coatings' contribution to accomplish intelligent infrastructure.

Acknowledgements

This project has received funding from the European Union's Horizon 2020 research and innovation programme under the Marie Skłodowska-Curie grant agreement No 860006.

References

[1] T. Hong, C. Koo, J. Kim, M. Lee, and K. Jeong, "A review on sustainable construction management strategies for monitoring, diagnosing, and retrofitting the building's dynamic energy performance: Focused on the operation and maintenance phase," *Appl. Energy*, vol. 155, pp. 671–707, 2015, doi: 10.1016/j.apenergy.2015.06.043.

[2] J. M. W. Brownjohn, "Structural health monitoring of civil infrastructure," *Philos. Trans. R. Soc. A Math. Phys. Eng. Sci.*, vol. 365, no. 1851, pp. 589–622, 2007, doi: 10.1098/rsta.2006.1925.

[3] K. Yan, Y. Zhang, Y. Yan, C. Xu, and S. Zhang, "Fault diagnosis method of sensors in building structural health monitoring system based on communication load optimization," *Comput. Commun.*, vol. 159, no. April, pp. 310–316, 2020, doi: 10.1016/j.comcom.2020.05.026.

[4] J. dos Reis, C. Oliveira Costa, and J. Sá da Costa, "Strain gauges debonding fault detection for structural health monitoring," *Struct. Control Heal. Monit.*, vol. 25, no. 12, pp. 1–14, 2018, doi: 10.1002/stc.2264.

[5] S. Ding, S. Dong, A. Ashour, and B. Han, "Development of sensing concrete: Principles, properties and its applications," *Journal of Applied Physics*, vol. 126, no. 24. American Institute of Physics Inc., Dec. 28, 2019. doi: 10.1063/1.5128242.

[6] J. Xu, W. Zhong, and W. Yao, "Modeling of conductivity in carbon fiber-reinforced cement-based composite," *J. Mater. Sci.*, vol. 45, no. 13, pp. 3538–3546, 2010, doi: 10.1007/s10853-010-4396-5.

[7] W. Dong, W. Li, Z. Tao, and K. Wang, "Piezoresistive properties of cement-based sensors: Review and perspective," *Construction and Building Materials*, vol. 203. Elsevier Ltd, pp. 146–163, Apr. 10, 2019. doi: 10.1016/j.conbuildmat.2019.01.081.

[8] A. D'Alessandro, H. B. Birgin, G. Cerni, and F. Ubertini, "Smart Infrastructure

Monitoring through Self-Sensing Composite Sensors and Systems: A Study on Smart Concrete Sensors with Varying Carbon-Based Filler," *Infrastructures*, vol. 7, no. 4, Apr. 2022, doi: 10.3390/infrastructures7040048.

[9] E. García-Macías, A. D'Alessandro, R. Castro-Triguero, D. Pérez-Mira, and F. Ubertini, "Micromechanics modeling of the uniaxial strain-sensing property of carbon nanotube cement-matrix composites for SHM applications," *Compos. Struct.*, vol. 163, pp. 195–215, Mar. 2017, doi: 10.1016/j.compstruct.2016.12.014.

[10] H. B. Birgin, A. D'alessandro, S. Laflamme, and F. Ubertini, "Smart graphite–cement composite for roadway-integrated weigh-in-motion sensing," *Sensors (Switzerland)*, vol. 20, no. 16, pp. 1–17, 2020, doi: 10.3390/s20164518.

[11] P. T. Dalla, K. G. Dassios, I. K. Tragazikis, D. A. Exarchos, and T. E. Matikas, "Carbon nanotubes and nanofibers as strain and damage sensors for smart cement," *Mater. Today Commun.*, vol. 8, pp. 196–204, 2016, doi: 10.1016/j.mtcomm.2016.07.004.

[12] S. K. T. Grattan, S. E. Taylor, P. A. M. Basheer, T. Sun, and K. T. V. Grattan, "Monitoring of Corrosion in Structural Reinforcing Bars: Performance Comparison Using In Situ Fiber-Optic and Electric Wire Strain Gauge Systems," *IEEE Sens. J.*, vol. 9, no. 11, pp. 1494–1502, 2009, doi: 10.1109/JSEN.2009.2019348.

[13] K. Zhang, B. Han, and X. Yu, "Nickel particle based electrical resistance heating cementitious composites," *Cold Reg. Sci. Technol.*, vol. 69, no. 1, pp. 64–69, 2011, doi: 10.1016/j.coldregions.2011.07.002.

[14] D. Wanasinghe, F. Aslani, and G. Ma, "Electromagnetic shielding properties of cementitious composites containing carbon nanofibers, zinc oxide, and activated carbon powder," *Constr. Build. Mater.*, vol. 285, p. 122842, 2021, doi: 10.1016/j.conbuildmat.2021.122842.

[15] B. J. Christensen *et al.*, "Impedance Spectroscopy of Hydrating Cement-Based Materials: Measurement, Interpretation, and Application," *J. Am. Ceram. Soc.*, vol. 77, no. 11, pp. 2789–2804, 1994, doi: 10.1111/j.1151-2916.1994.tb04507.x.

[16] B. Chen, K. Wu, and W. Yao, "Conductivity of carbon fiber reinforced cement-based composites," *Cem. Concr. Compos.*, vol. 26, no. 4, pp. 291–297, 2004, doi: 10.1016/S0958-9465(02)00138-5.

[17] M. Nagao, K. Kobayashi, T. Hori, Y. Li, and T. Hibino, "Humidity driven transition from insulator to ionic conductor in Portland cement," *Materials (Basel).*, vol. 12, no. 22, 2019, doi: 10.3390/ma12223701.

[18] Q. Chang, *Colloid and Interface Chemistry for Water Quality Control*. John Fedor, 2016.

[19] S. Wen and D. D. L. Chung, "Effect of moisture on piezoresistivity of carbon fiber-reinforced cement paste," *ACI Mater. J.*, vol. 105, no. 3, pp. 274–280, 2008, doi: 10.14359/19824.

[20] B. Nettelblad and G. A. Niklasson, "Dielectric relaxations in liquid-impregnated porous solids," *J. Mater. Sci.*, vol. 32, no. 14, pp. 3783–3800, 1997, doi: 10.1023/A:1018675607187.

[21] J. Zhang, A. Heath, H. M. T. Abdalgadir, R. J. Ball, and K. Paine, "Electrical impedance behaviour of carbon fibre reinforced cement-based sensors at different moisture

contents," *Constr. Build. Mater.*, vol. 353, Oct. 2022, doi: 10.1016/j.conbuildmat.2022.129049.

[22] B. Han, X. Yu, E. Kwon, and J. Ou, "Effects of CNT concentration level and water/cement ratio on the piezoresistivity of CNT/cement composites," *J. Compos. Mater.*, vol. 46, no. 1, pp. 19–25, 2012, doi: 10.1177/0021998311401114.

[23] M. F. Islam, E. Rojas, D. M. Bergey, A. T. Johnson, and A. G. Yodh, "High weight fraction surfactant solubilization of single-wall carbon nanotubes in water," *Nano Lett.*, vol. 3, no. 2, pp. 269–273, 2003, doi: 10.1021/nl025924u.

[24] W. Dong, W. Li, N. Lu, F. Qu, K. Vessalas, and D. Sheng, "Piezoresistive behaviours of cement-based sensor with carbon black subjected to various temperature and water content," *Compos. Part B Eng.*, vol. 178, no. September, 2019, doi: 10.1016/j.compositesb.2019.107488.

[25] B. del Moral *et al.*, "Temperature and humidity influence on the strain sensing performance of hybrid carbon nanotubes and graphite cement composites," *Constr. Build. Mater.*, vol. 284, May 2021, doi: 10.1016/j.conbuildmat.2021.122786.

[26] B. Han, X. Yu, and J. Ou, "Effect of water content on the piezoresistivity of MWNT/cement composites," *J. Mater. Sci.*, vol. 45, no. 14, pp. 3714–3719, 2010, doi: 10.1007/s10853-010-4414-7.

[27] Y. Kim, S.-Y. Seo, H.-D. Yun, L. Gun-Cheol, and S. Hong, "Development and Investigation of Repair Self-Sensing Composites Using S-CNT," *Buildings*, 2023, doi: 10.3390/buildings13041015.

[28] J. Luo *et al.*, "Influences of multi-walled carbon nanotube (MCNT) fraction, moisture, stress/strain level on the electrical properties of MCNT cement-based composites," *Sensors Actuators, A Phys.*, vol. 280, pp. 413–421, Sep. 2018, doi: 10.1016/j.sna.2018.08.010.

[29] E. Teomete, "The effect of temperature and moisture on electrical resistance, strain sensitivity and crack sensitivity of steel fiber reinforced smart cement composite," *Smart Mater. Struct.*, vol. 25, no. 7, Jun. 2016, doi: 10.1088/0964-1726/25/7/075024.

[30] H. Wang *et al.*, "Electrical and piezoresistive properties of carbon nanofiber cement mortar under different temperatures and water contents," *Constr. Build. Mater.*, vol. 265, p. 120740, 2020, doi: 10.1016/j.conbuildmat.2020.120740.

[31] C. Song and S. Choi, "Moisture-dependent piezoresistive responses of CNT-embedded cementitious composites," *Compos. Struct.*, vol. 170, pp. 103–110, Jun. 2017, doi: 10.1016/j.compstruct.2017.03.009.

[32] E. Demircilioğlu, E. Teomete, E. Schlangen, and F. J. Baeza, "Temperature and moisture effects on electrical resistance and strain sensitivity of smart concrete," *Constr. Build. Mater.*, vol. 224, pp. 420–427, Nov. 2019, doi: 10.1016/j.conbuildmat.2019.07.091.

[33] S. H. Jang, D. P. Hochstein, S. Kawashima, and H. Yin, "Experiments and micromechanical modeling of electrical conductivity of carbon nanotube/cement composites with moisture," *Cem. Concr. Compos.*, vol. 77, pp. 49–59, Mar. 2017, doi: 10.1016/j.cemconcomp.2016.12.003.

[34] D. D. L. Chung, "A critical review of electrical-resistance-based self-sensing in conductive cement-based materials," *Carbon N. Y.*, vol. 203, no. August 2022, pp. 311–

844 325, 2023, doi: 10.1016/j.carbon.2022.11.076.

845 [35] L. Qiu, L. Li, A. Ashour, S. Ding, and B. Han, "Monitoring damage of concrete beams
846 via self-sensing cement mortar coating with carbon nanotube-nano carbon black
847 composite fillers," *J. Intell. Mater. Syst. Struct.*, no. 3, 2024, doi:
848 10.1177/1045389X231221129.

849 [36] S. Ding, Y. Ruan, X. Yu, B. Han, and Y. Q. Ni, "Self-monitoring of smart concrete
850 column incorporating CNT/NCB composite fillers modified cementitious sensors,"
851 *Constr. Build. Mater.*, vol. 201, pp. 127–137, 2019, doi:
852 10.1016/j.conbuildmat.2018.12.203.

853 [37] K. Soga and L. Luo, "Distributed fiber optics sensors for civil engineering infrastructure
854 sensing," *J. Struct. Integr. Maint.*, vol. 3, no. 1, pp. 1–21, 2018, doi:
855 10.1080/24705314.2018.1426138.

856 [38] B. Han and J. Ou, "Embedded piezoresistive cement-based stress/strain sensor," *Sensors
857 Actuators, A Phys.*, vol. 138, no. 2, pp. 294–298, 2007, doi: 10.1016/j.sna.2007.05.011.

858 [39] C. Vlachakis, X. Wang, and A. Al-Tabbaa, "Investigation of the compressive self-
859 sensing response of filler-free metakaolin geopolymer binders and coatings," *Constr.
860 Build. Mater.*, vol. 392, no. June, p. 131682, 2023, doi:
861 10.1016/j.conbuildmat.2023.131682.

862 [40] J. McAlorum, M. Perry, A. C. Ward, and C. Vlachakis, "Concreits: An electrical
863 impedance interrogator for concrete damage detection using self-sensing repairs,"
864 *Sensors*, vol. 21, no. 21, 2021, doi: 10.3390/s21217081.

865 [41] T. Manzur, N. Yazdani, and M. A. B. Emon, "Potential of carbon nanotube reinforced
866 cement composites as concrete repair material," *J. Nanomater.*, vol. 2016, 2016, doi:
867 10.1155/2016/1421959.

868 [42] B. Díaz, B. Guitián, X. R. Nóvoa, and C. Pérez, "Conductivity assessment of
869 multifunctional cement pastes by impedance spectroscopy," *Corros. Sci.*, vol. 185, no.
870 March, 2021, doi: 10.1016/j.corsci.2021.109441.

871 [43] S. Wen and D. D. L. Chung, "The role of electronic and ionic conduction in the electrical
872 conductivity of carbon fiber reinforced cement," *Carbon N. Y.*, vol. 44, no. 11, pp. 2130–
873 2138, 2006, doi: 10.1016/j.carbon.2006.03.013.

874 [44] P. Garcés, E. Zornoza, E. G. Alcocel, Ó. Galao, and L. G. Andión, "Mechanical
875 properties and corrosion of CAC mortars with carbon fibers," *Constr. Build. Mater.*, vol.
876 34, pp. 91–96, 2012, doi: 10.1016/j.conbuildmat.2012.02.020.

877 [45] M. Uysal, K. Yilmaz, and M. Ipek, "The effect of mineral admixtures on mechanical
878 properties, chloride ion permeability and impermeability of self-compacting concrete,"
879 *Constr. Build. Mater.*, vol. 27, no. 1, pp. 263–270, 2012, doi:
880 10.1016/j.conbuildmat.2011.07.049.

881 [46] Y. Zha, J. Yu, R. Wang, P. He, and Z. Cao, "Effect of ion chelating agent on self-healing
882 performance of Cement-based materials," *Constr. Build. Mater.*, vol. 190, pp. 308–316,
883 2018, doi: 10.1016/j.conbuildmat.2018.09.115.

884 [47] H. Li, H. gang Xiao, and J. ping Ou, "Effect of compressive strain on electrical resistivity
885 of carbon black-filled cement-based composites," *Cem. Concr. Compos.*, vol. 28, no. 9,
886 pp. 824–828, Oct. 2006, doi: 10.1016/j.cemconcomp.2006.05.004.

887 [48] M. A. Haynes, E. Coleri, and I. Obaid, "Performance of waterproofing membranes to
888 protect concrete bridge decks," in *Transportation Research Record*, vol. 2675, no. 9,
889 SAGE Publications Ltd, 2021, pp. 1693–1706. doi: 10.1177/03611981211009527.

890 [49] W. Dong, W. Li, Y. Guo, F. Qu, K. Wang, and D. Sheng, "Piezoresistive performance
891 of hydrophobic cement-based sensors under moisture and chloride-rich environments,"
892 *Cem. Concr. Compos.*, vol. 126, no. November 2021, p. 104379, 2022, doi:
893 10.1016/j.cemconcomp.2021.104379.

894 [50] H. Li, H. Xiao, and J. Ou, "Electrical property of cement-based composites filled with
895 carbon black under long-term wet and loading condition," *Compos. Sci. Technol.*, vol.
896 68, no. 9, pp. 2114–2119, Jul. 2008, doi: 10.1016/j.compscitech.2008.03.007.

897 [51] A. O. Monteiro, P. M. F. J. Costa, M. Oeser, and P. B. Cachim, "Dynamic sensing
898 properties of a multifunctional cement composite with carbon black for traffic
899 monitoring," *Smart Mater. Struct.*, vol. 29, no. 2, 2020, doi: 10.1088/1361-
900 665X/ab62e2.

901 [52] S. Y. Guo, H. H. Luo, Z. Tan, J. Z. Chen, L. Zhang, and J. Ren, "Impermeability and
902 interfacial bonding strength of TiO2-graphene modified epoxy resin coated OPC
903 concrete," *Prog. Org. Coatings*, vol. 151, no. October 2020, p. 106029, 2021, doi:
904 10.1016/j.porgcoat.2020.106029.

905 [53] C. Li, H. Ge, D. Sun, and X. Zhou, "Novel conductive wearing course using a graphite,
906 carbon fiber, and epoxy resin mixture for active de-icing of asphalt concrete pavement,"
907 *Mater. Struct. Constr.*, vol. 54, no. 1, Feb. 2021, doi: 10.1617/s11527-021-01628-7.

908 [54] K. Subrahmanya, K. Vadivuchezhian, and N. Chockappan, "Experimental Verification
909 of Effect of Adhesive Layer Thickness Used for Strain Gauge Mounting," *Adv. Mater.*
910 *Res.*, vol. 1119, pp. 789–793, 2015, doi: 10.4028/www.scientific.net/amr.1119.789.

911 [55] F. Djouani, C. Connan, M. Delamar, M. M. Chehimi, and K. Benzarti, "Cement paste-
912 epoxy adhesive interactions," *Constr. Build. Mater.*, vol. 25, no. 2, pp. 411–423, 2011,
913 doi: 10.1016/j.conbuildmat.2010.02.035.

914 [56] E. Komurlu, F. Cihangir, A. Kesimal, and S. Demir, "Effect of Adhesive Type on the
915 Measurement of Modulus of Elasticity Using Electrical Resistance Strain Gauges,"
916 *Arab. J. Sci. Eng.*, vol. 41, no. 2, pp. 433–441, 2016, doi: 10.1007/s13369-015-1837-0.

917 [57] M. Amjadi, K. U. Kyung, I. Park, and M. Sitti, "Stretchable, Skin-Mountable, and
918 Wearable Strain Sensors and Their Potential Applications: A Review," *Adv. Funct.*
919 *Mater.*, vol. 26, no. 11, pp. 1678–1698, 2016, doi: 10.1002/adfm.201504755.

920 [58] A. Nag, M. E. E. Alahi, S. C. Mukhopadhyay, and Z. Liu, "Multi-walled carbon
921 nanotubes-based sensors for strain sensing applications," *Sensors (Switzerland)*, vol. 21,
922 no. 4, pp. 1–22, 2021, doi: 10.3390/s21041261.

923 [59] "BS EN 197-1:2011; Cement—Part 1: Composition, Specifications and Conformity
924 Criteria for Common Cements." British Standards Institutions, London, UK, 2011.

925 [60] "BS EN 206-1:2013; Concrete—Specification, Performance, Production, and
926 Conformity." British Standards Institutions, London, UK, 2013.

927 [61] V. Afroughsabet and A. Al-tabbaa, "Effect of SAPs and polypropylene fibres on the
928 freeze-thaw resistance of low carbon roller compacted concrete pavement," vol. 08006,
929 pp. 1–6, 2023, doi: 10.1051/matecconf/202337808006.

[62] "BS EN 12390-1:2012; Testing Hardened Concrete—Part 1: Shape, Dimensions and Other Requirements for Specimens and Moulds." British Standards Institutions, London, UK, 2012.

[63] A. D. Espeche and J. León, "Estimation of bond strength envelopes for old-to-new concrete interfaces based on a cylinder splitting test," *Constr. Build. Mater.*, vol. 25, no. 3, pp. 1222–1235, 2011, doi: 10.1016/j.conbuildmat.2010.09.032.

[64] M. Tabatabaei, A. Dahi Taleghani, and N. Alem, "Nanoengineering of cement using graphite platelets to refine inherent microstructural defects," *Compos. Part B Eng.*, vol. 202, no. February, p. 108277, 2020, doi: 10.1016/j.compositesb.2020.108277.

[65] A. Momayez, M. R. Ehsani, A. A. Ramezanianpour, and H. Rajaie, "Comparison of methods for evaluating bond strength between concrete substrate and repair materials," *Cem. Concr. Res.*, vol. 35, no. 4, pp. 748–757, 2005, doi: 10.1016/j.cemconres.2004.05.027.

[66] L. F. M. da Silva, T. N. S. S. Rodrigues, M. A. V. Figueiredo, M. F. S. F. de Moura, and J. A. G. Chousal, "Effect of adhesive type and thickness on the lap shear strength," *J. Adhes.*, vol. 82, no. 11, pp. 1091–1115, 2006, doi: 10.1080/00218460600948511.

[67] G. Milone, C. Vlachakis, J. M. Tulliani, and A. Al-Tabbaa, "Strain Monitoring of Concrete Using Carbon Black-Based Smart Coatings," *Materials (Basel).*, vol. 17, no. 7, 2024, doi: 10.3390/ma17071577.

[68] S. Wen and D. D. L. Chung, "Carbon fiber-reinforced cement as a strain-sensing coating," *Cem. Concr. Res.*, vol. 31, no. 4, pp. 665–667, 2001, doi: 10.1016/S0008-8846(01)00474-4.

[69] "BS EN 1992-1-1:2004; Design of Concrete Structures—Part 1-1: General Rules and Rules for Buildings." British Standards Institutions, London, UK, 2004.

[70] "BS EN 998-1:2016; Specification for mortar for masonry - Rendering and plastering mortar." British Standards Institutions, London, UK, 2016.

[71] P. Wang, Q. Yang, Z. Jin, D. Hou, and M. Wang, "Effects of water and ions on bonding behavior between epoxy and hydrated calcium silicate: a molecular dynamics simulation study," *J. Mater. Sci.*, vol. 56, no. 29, pp. 16475–16490, 2021, doi: 10.1007/s10853-021-06374-3.

[72] P. Gujar, A. Alex, M. Santhanam, and P. Ghosh, "Evaluation of interfacial strength between hydrating cement paste and epoxy coating," *Constr. Build. Mater.*, vol. 279, p. 122511, 2021, doi: 10.1016/j.conbuildmat.2021.122511.

[73] D. Smyl, F. Ghasemzadeh, and M. Pour-Ghaz, "Modeling water absorption in concrete and mortar with distributed damage," *Constr. Build. Mater.*, vol. 125, pp. 438–449, 2016, doi: 10.1016/j.conbuildmat.2016.08.044.

[74] J. Castro, D. Bentz, and J. Weiss, "Effect of sample conditioning on the water absorption of concrete," *Cem. Concr. Compos.*, vol. 33, no. 8, pp. 805–813, 2011, doi: 10.1016/j.cemconcomp.2011.05.007.

[75] W. Zhao, Y. Jiang, Y. Yu, and W. Liu, "Use of digital image correlation to confirm the enhancement of concrete–epoxy resin mortar adhesion through surface precoating treatment," *Constr. Build. Mater.*, vol. 295, p. 123512, 2021, doi: 10.1016/j.conbuildmat.2021.123512.

973 [76] A. Szewczak and G. Łagód, "Adhesion of Modified Epoxy Resin to a Concrete Surface,"
974 *Materials (Basel).*, vol. 15, no. 24, 2022, doi: 10.3390/ma15248961.

975 [77] J. K. Park and M. O. Kim, "The effect of different exposure conditions on the pull-off
976 strength of various epoxy resins," *J. Build. Eng.*, vol. 38, no. October 2020, p. 102223,
977 2021, doi: 10.1016/j.jobe.2021.102223.

978 [78] E. Ozeren Ozgul and M. H. Ozkul, "Effects of epoxy, hardener, and diluent types on the
979 hardened state properties of epoxy mortars," *Constr. Build. Mater.*, vol. 187, pp. 360–
980 370, 2018, doi: 10.1016/j.conbuildmat.2018.07.215.

981 [79] "BS EN 13670:2009; Execution of Concrete Structures." British Standards Institutions,
982 London, UK, 2009.

983 [80] "BS 8500:2020; Concrete—Complementary British Standard to BS EN 206." British
984 Standards Institutions, London, UK, 2020.

985 [81] "BS EN 12390-6:2009; Testing Hardened Concrete—Part 6: Tensile Splitting Strength
986 of Test Specimens." British Standards Institutions, London, UK, 2009.

987 [82] X. Li, Z. C. Grasley, J. W. Bullard, and E. J. Garboczi, "Irreversible desiccation
988 shrinkage of cement paste caused by cement grain dissolution and hydrate
989 precipitation," *Mater. Struct. Constr.*, vol. 50, no. 2, pp. 1–14, 2017, doi:
990 10.1617/s11527-016-0974-6.

991 [83] J. Zuo, W. Yao, and K. Wu, "Seebeck effect and mechanical properties of carbon
992 nanotube-carbon fiber/cement nanocomposites," *Fullerenes Nanotub. Carbon*
993 *Nanostructures*, vol. 23, no. 5, pp. 383–391, 2015, doi:
994 10.1080/1536383X.2013.863760.

995 [84] Y. Zhang, X. Ouyang, and Z. Yang, "Microstructure-based relative humidity in
996 cementitious system due to self-desiccation," *Materials (Basel).*, vol. 12, no. 8, pp. 1–
997 15, 2019, doi: 10.3390/ma12081214.

998 [85] X. Tian and H. Hu, "Test and Study on Electrical Property of Conductive Concrete,"
999 *Procedia Earth Planet. Sci.*, vol. 5, pp. 83–87, 2012, doi: 10.1016/j.proeps.2012.01.014.

1000 [86] F. Reza, G. B. Batson, J. A. Yamamuro, and J. S. Lee, "Resistance Changes during
1001 Compression of Carbon Fiber Cement Composites," *J. Mater. Civ. Eng.*, vol. 15, no. 5,
1002 pp. 476–483, 2003, doi: 10.1061/(asce)0899-1561(2003)15:5(476).

1003 [87] A. C. Lazanas and M. I. Prodromidis, "Electrochemical Impedance Spectroscopy─A
1004 Tutorial," *ACS Meas. Sci. Au*, vol. 3, no. 3, pp. 162–193, 2023, doi:
1005 10.1021/acsmeasuresciau.2c00070.

1006 [88] I. Papanikolaou, C. Litina, A. Zomorodian, and A. Al-Tabbaa, "Effect of natural
1007 graphite fineness on the performance and electrical conductivity of cement paste mixes
1008 for self-sensing structures," *Materials (Basel).*, vol. 13, no. 24, pp. 1–19, Dec. 2020, doi:
1009 10.3390/ma13245833.

1010 [89] M. Frąc, W. Szudek, P. Szołdra, and W. Pichór, "The applicability of shungite as an
1011 electrically conductive additive in cement composites," *J. Build. Eng.*, vol. 45, no.
1012 September 2021, pp. 1–10, 2022, doi: 10.1016/j.jobe.2021.103469.

1013 [90] B. Han, S. Ding, and X. Yu, "Intrinsic self-sensing concrete and structures: A review,"
1014 *Measurement: Journal of the International Measurement Confederation*, vol. 59.

Elsevier B.V., pp. 110–128, 2015. doi: 10.1016/j.measurement.2014.09.048.

[91] D. G. Meehan, Shoukai Wang, and D. D. L. Chung, "Electrical-resistance-based sensing of impact damage in carbon fiber reinforced cement-based materials," *J. Intell. Mater. Syst. Struct.*, vol. 21, no. 1, pp. 83–105, Jan. 2010, doi: 10.1177/1045389X09354786.

[92] S. A. Stanier, J. Blaber, W. A. Take, and D. J. White, "Improved image-based deformation measurement for geotechnical applications," *Can. Geotech. J.*, vol. 53, no. 5, pp. 727–739, 2016, doi: 10.1139/cgj-2015-0253.

[93] Y. Guo *et al.*, "Self-sensing performance of cement-based sensor with carbon black and polypropylene fibre subjected to different loading conditions," *J. Build. Eng.*, vol. 59, no. July, p. 105003, 2022, doi: 10.1016/j.jobe.2022.105003.

[94] S. Shoukry *et al.*, "Effect of Moisture and Temperature on the Mechanical Properties of Concrete Brian Downie Thesis submitted to the College of Engineering and Mineral Resources at West Virginia University in partial fulfillment of the requirements for the degree of Master o," *Time*, 2005.

[95] J. R. Macdonald and E. Barsoukov, *Impedance spectroscopy: theory experiment, and applications*. John Wiley and Sons Inc., 2018.

[96] B. Díaz, B. Guitián, X. R. Nóvoa, and C. Pérez, "Analysis of the microstructure of carbon fibre reinforced cement pastes by impedance spectroscopy," *Constr. Build. Mater.*, vol. 243, 2020, doi: 10.1016/j.conbuildmat.2020.118207.

[97] W. Dong, W. Li, K. Wang, B. Han, D. Sheng, and S. P. Shah, "Investigation on physicochemical and piezoresistive properties of smart MWCNT/cementitious composite exposed to elevated temperatures," *Cem. Concr. Compos.*, vol. 112, no. April, p. 103675, 2020, doi: 10.1016/j.cemconcomp.2020.103675.

[98] H. F. Taylor, "A method for predicting alkazi ion concentrations in cement pore solutions," *Adv. Cem. Res.*, vol. 1, no. 1, pp. 5–17, 1987, doi: doi.org/10.1680/adcr.1987.1.1.5.

[99] J. Zhang, A. Heath, H. M. T. Abdalgadir, R. J. Ball, and K. Paine, "Electrical impedance behaviour of carbon fibre reinforced cement-based sensors at different moisture contents," *Constr. Build. Mater.*, vol. 353, no. May, p. 129049, 2022, doi: 10.1016/j.conbuildmat.2022.129049.

[100] J. M. Torrents, T. O. Mason, and E. J. Garboczi, "Impedance spectra of fiber-reinforced cement-based composites: A modeling approach," *Cem. Concr. Res.*, vol. 30, no. 4, pp. 585–592, 2000, doi: 10.1016/S0008-8846(00)00211-8.

[101] J. M. Torrents, T. O. Mason, A. Peled, S. P. Shah, and E. J. Garboczi, "Analysis of the impedance spectra of short conductive fiber-reinforced composites," *J. Mater. Sci.*, vol. 36, no. 16, pp. 4003–4012, 2001, doi: 10.1023/A:1017986608910.

[102] W. J. McCarter, G. Starrs, T. M. Chrisp, and P. F. G. Banfill, "Complex impedance and dielectric dispersion in carbon fiber reinforced cement matrices," *J. Am. Ceram. Soc.*, vol. 92, no. 7, pp. 1617–1620, 2009, doi: 10.1111/j.1551-2916.2009.03057.x.

[103] G. Song, "Equivalent circuit model for AC electrochemical impedance spectroscopy of concrete," *Cem. Concr. Res.*, vol. 30, no. 11, pp. 1723–1730, 2000, doi: 10.1016/S0008-8846(00)00400-2.

[104] W. J. McCarter and R. Brousseau, "The A.C. response of hardened cement paste," *Cem. Concr. Res.*, vol. 20, no. 6, pp. 891–900, 1990, doi: 10.1016/0008-8846(90)90051-X.

[105] G. Y. Li, P. M. Wang, and X. Zhao, "Pressure-sensitive properties and microstructure of carbon nanotube reinforced cement composites," *Cem. Concr. Compos.*, vol. 29, no. 5, pp. 377–382, May 2007, doi: 10.1016/j.cemconcomp.2006.12.011.

[106] S. Bai, L. Jiang, Y. Jiang, M. Jin, S. Jiang, and D. Tao, "Research on electrical conductivity of graphene/cement composites," *Adv. Cem. Res.*, vol. 32, no. 2, pp. 45–52, Feb. 2020, doi: 10.1680/jadcr.16.00170.

[107] L. A. Modesti, A. S. de Vargas, and E. L. Schneider, "Repairing concrete with epoxy adhesives," *Int. J. Adhes. Adhes.*, vol. 101, no. May, p. 102645, 2020, doi: 10.1016/j.ijadhadh.2020.102645.

[108] "BS EN 1504-3:2005; Products and Systems for the Protection and Repair of Concrete Structures—Definitions, Requirements, Quality Control and Evaluation of Conformity—Part 3: Structural and Non-Structural Repair." British Standards Institutions, London, UK, 2005.

[109] E. Gomaa, A. Gheni, and M. A. ElGawady, "Repair of ordinary Portland cement concrete using ambient-cured alkali-activated concrete: Interfacial behavior," *Cem. Concr. Res.*, vol. 129, no. June 2019, p. 105968, 2020, doi: 10.1016/j.cemconres.2019.105968.

[110] Y. Bai, P. A. M. Basheer, D. J. Cleland, and A. E. Long, "State-of-the-art applications of the pull-off test in civil engineering," *Int. J. Struct. Eng.*, vol. 1, no. 1, pp. 93–103, 2009, doi: https://doi.org/10.1504/IJStructE.2009.030028.

[111] M. Frigione, M. A. Aiello, and C. Naddeo, "Water effects on the bond strength of concrete/concrete adhesive joints," *Constr. Build. Mater.*, vol. 20, no. 10, pp. 957–970, 2006, doi: 10.1016/j.conbuildmat.2005.06.015.

[112] L. Tu and D. Kruger, "Engineering Properties of Epoxy Resins Used as Concrete Adhesives," *Mater. J.*, vol. 93, no. 1, pp. 26–35, 1996, doi: 10.14359/9793.

[113] C. Vlachakis, Y. F. Su, X. Wang, and A. Al-Tabbaa, "Mechanics-perspective evaluation of self-sensing geopolymer coatings in structural health monitoring," *Dev. Built Environ.*, vol. 18, no. February, p. 100387, 2024, doi: 10.1016/j.dibe.2024.100387.

[114] K. Rashid, T. Ueda, D. Zhang, K. Miyaguchi, and H. Nakai, "Experimental and analytical investigations on the behavior of interface between concrete and polymer cement mortar under hygrothermal conditions," *Constr. Build. Mater.*, vol. 94, pp. 414–425, 2015, doi: 10.1016/j.conbuildmat.2015.07.035.

[115] Y. Yin and Y. Fan, "Influence of roughness on shear bonding performance of CFRP-concrete interface," *Materials (Basel).*, vol. 11, no. 10, pp. 1–15, 2018, doi: 10.3390/ma11101875.

[116] Q. Luo, T. Qin, Z. Chen, B. Pang, J. Qu, and Z. Gao, "The influence of moisture and epoxy bonding agents on interfacial behavior between normal concrete substrate and ultrahigh performance concrete as a repair material: Experimental and molecular dynamics study," *Constr. Build. Mater.*, vol. 372, no. October 2022, p. 130779, 2023, doi: 10.1016/j.conbuildmat.2023.130779.

[117] J. Yu, S. Li, D. Hou, Z. Jin, and Q. Liu, "Hydrophobic silane coating films for the

1100 inhibition of water ingress into the nanometer pore of calcium silicate hydrate gels,"
1101 *Phys. Chem. Chem. Phys.*, vol. 21, no. 35, pp. 19026–19038, 2019, doi:
1102 10.1039/c9cp03266e.

1103 [118] J. Chen, Y. Zhang, D. Hou, J. Yu, T. Zhao, and B. Yin, "Experiment and molecular
1104 dynamics study on the mechanism for hydrophobic impregnation in cement-based
1105 materials: A case of octadecane carboxylic acid," *Constr. Build. Mater.*, vol. 229, p.
1106 116871, 2019, doi: 10.1016/j.conbuildmat.2019.116871.

1107 [119] A. A. Bahraq, M. A. Al-Osta, O. S. B. Al-Amoudi, T. A. Saleh, and I. B. Obot,
1108 "Atomistic simulation of polymer-cement interactions: Progress and research
1109 challenges," *Constr. Build. Mater.*, vol. 327, no. February, p. 126881, 2022, doi:
1110 10.1016/j.conbuildmat.2022.126881.

1111 [120] V. Ambrogi, C. Carfagna, P. Cerruti, and V. Marturano, *Additives in Polymers*. Elsevier
1112 Inc., 2017. doi: 10.1016/B978-0-323-44353-1.00004-X.

1113 [121] H. A. Al-Turaif, "Surface morphology and chemistry of epoxy-based coatings after
1114 exposure to ultraviolet radiation," *Prog. Org. Coatings*, vol. 76, no. 4, pp. 677–681,
1115 2013, doi: 10.1016/j.porgcoat.2012.12.010.

1116 [122] A. Krzyzak, D. Racinowski, R. Szczepaniak, M. Mucha, and E. Kosicka, "The impact
1117 of selected atmospheric conditions on the process of abrasive wear of CFRP," *Materials
1118 (Basel).*, vol. 13, no. 18, 2020, doi: 10.3390/ma13183965.

1119 [123] M. Sarker, S. A. Hadigheh, and D. Dias-da-Costa, "A performance-based
1120 characterisation of CFRP composite deterioration using active infrared thermography,"
1121 *Compos. Struct.*, vol. 241, no. February, p. 112134, 2020, doi:
1122 10.1016/j.compstruct.2020.112134.

1123 [124] I. Alj *et al.*, "Experimental and numerical investigation on the strain response of
1124 distributed optical fiber sensors bonded to concrete: Influence of the adhesive stiffness
1125 on crack monitoring performance," *Sensors (Switzerland)*, vol. 20, no. 18, pp. 1–24,
1126 2020, doi: 10.3390/s20185144.

1127 [125] X. Li and M. Li, "Multifunctional self-sensing and ductile cementitious materials," *Cem.
1128 Concr. Res.*, vol. 123, no. July, 2019, doi: 10.1016/j.cemconres.2019.03.008.

1129 [126] G. H. Nalon *et al.*, "Effects of different kinds of carbon black nanoparticles on the
1130 piezoresistive and mechanical properties of cement-based composites," *J. Build. Eng.*,
1131 vol. 32, Nov. 2020, doi: 10.1016/j.jobe.2020.101724.

1132 [127] L. Wittocx *et al.*, "Piezoelectricity-based self-sensing of compressive and flexural stress
1133 in cement-based materials without admixture requirement and without poling," *Constr.
1134 Build. Mater.*, vol. 27, no. 10, pp. 671–707, Jan. 2022, doi: 10.1016/j.jobe.2022.104436.

1135 [128] W. Dong, W. Li, K. Wang, S. P. Shah, and D. Sheng, "Multifunctional cementitious
1136 composites with integrated self-sensing and self-healing capacities using carbon black
1137 and slaked lime," *Ceram. Int.*, vol. 48, no. 14, pp. 19851–19863, Jul. 2022, doi:
1138 10.1016/j.ceramint.2022.03.260.

1139 [129] F. J. Baeza, O. Galao, E. Zornoza, and P. Garcés, "Multifunctional cement composites
1140 strain and damage sensors applied on reinforced concrete (RC) structural elements,"
1141 *Materials (Basel).*, vol. 6, no. 3, pp. 841–855, 2013, doi: 10.3390/ma6030841.

1142 [130] R. Durairaj, T. Varatharajan, S. K. Srinivasan, B. G. A. Gurupatham, and K. Roy,

"Experimental Investigation on Flexural Behaviour of Sustainable Reinforced Concrete Beam with a Smart Mortar Layer," *J. Compos. Sci.*, vol. 7, no. 4, 2023, doi: 10.3390/jcs7040132.

[131] P. Yang, S. Chowdhury, and N. Neithalath, "Strain sensing ability of metallic particulate reinforced cementitious composites: Experiments and microstructure-guided finite element modeling," *Cem. Concr. Compos.*, vol. 90, pp. 225–234, Jul. 2018, doi: 10.1016/j.cemconcomp.2018.04.004.